Journal of Cosmology and Astroparticle Physics
An IOP and SISSA journal

A generalized local ansatz and its effect on halo bias

Sarah Shandera,[a] **Neal Dalal**[b] **and Dragan Huterer**[c]

[a]Perimeter Institute for Theoretical Physics,
Waterloo, Ontario, Canada
[b]Canadian Institute for Theoretical Astrophysics, University of Toronto,
Toronto, Ontario, Canada
[c]Department of Physics, University of Michigan,
Ann Arbor, Michigan, U.S.A.

E-mail: sshandera@perimeterinstitute.ca, neal@cita.utoronto.ca,
huterer@umich.edu

Received November 10, 2010
Revised February 9, 2011
Accepted February 26, 2011
Published March 7, 2011

Abstract. Motivated by the properties of early universe scenarios that produce observationally large local non-Gaussianity, we perform N-body simulations with non-Gaussian initial conditions from a generalized local ansatz. The bispectra are schematically of the local shape, but with scale-dependent amplitude. We find that in such cases the size of the non-Gaussian correction to the bias of small and large mass objects depends on the amplitude of non-Gaussianity roughly on the scale of the object. In addition, some forms of the generalized bispectrum alter the scale dependence of the non-Gaussian term in the bias by a fractional power of k. These features may allow significant observational constraints on the particle physics origin of any observed local non-Gaussianity, distinguishing between scenarios where a single field or multiple fields contribute to the curvature fluctuations. While analytic predictions for the non-Gaussian bias agree qualitatively with the simulations, we find numerically a stronger observational signal than expected. This suggests that a more precise understanding of halo formation is needed to fully explain the consequences of primordial non-Gaussianity.

Keywords: non-gaussianity, cosmological simulations, inflation

ArXiv ePrint: 1010.3722

doi:10.1088/1475-7516/2011/03/017

JCAP03(2011)017

Contents

1 Motivation

Non-Gaussianity that originates from the inflationary epoch leaves distinct signatures in present-day astrophysical measurements, and therefore provides a unique link to the early universe. Interactions of the field(s) sourcing the primordial curvature fluctuations introduce non-Gaussian imprints in the statistics of the temperature fluctuations in the Cosmic Microwave Background (CMB) and of the density fluctuations that collapse into bound objects. These effects give us many independent probes of the signals of inflationary physics at different redshifts, sensitive to a range of scales. While current measurements from the CMB confirm that the spectrum of primordial fluctuations is Gaussian to a remarkable part in 10^3, that bound is still four orders of magnitude away from testing primordial non-Gaussianity at the level predicted by slow-roll inflation and more than one order of magnitude above the level expected from non-linear post-inflationary processing of the fluctuations (see eg [1] for a recent calculation). In addition, *any* deviation from the simplest single field slow-roll inflationary scenario, including multiple fields, derivative interactions, features in the potential, or non-Bunch-Davies initial conditions (see [2] for a summary) can lead to observable non-Gaussianity at levels within current constraints but well above the slow-roll prediction. Upcoming data from the Planck satellite [3] and a variety of galaxy surveys [4–9] have the potential to achieve accuracy on non-Gaussianity at the level expected from non-linear evolution alone. For recent reviews, see [10–14].

Primordial non-Gaussianity is most effectively constrained by complementary measurements from the CMB and Large Scale Structure (LSS). The galaxy power spectrum and bispectrum and cluster number counts provide independent statistics with different systematics, sensitive to different qualitative features of the primordial non-Gaussianity. Combined

JCAP03(2011)017

with the CMB, these observations will constrain a wide range of qualitative features of any observed non-Gaussianity (including amplitude, shape, sign and scale dependence) which can rule out large classes of inflationary models.

Non-Gaussianity of the local type (with bispectrum maximum in the squeezed limit; $k_1 \approx k_2 \gg k_3$) has recently generated a good deal of interest in part because it will be especially well-constrained by LSS observations [15]. Even in the case of Gaussian fluctuations, the statistics of collapsed objects are different from those of the underlying density field, and the ratio of the clustering of the two is known as the halo bias [16]. The particular coupling of long and short wavelength modes in local non-Gaussianity introduces an additional, distinctive correction (proportional to $1/k^2$) in the power spectrum of collapsed objects which will allow strong observational constraints on local non-Gaussianity [15, 17, 18]. From a theoretical point of view, observably large primordial non-Gaussianity of this type *requires* at least two fields to contribute to the scenario - single field inflation alone can only generate a bispectrum of the local shape with an extremely small amplitude (of order the spectral index of the primordial power spectrum [19]). The complete phenomenology of multi-field models is rich but we will show here that there *are* qualitative differences that are observationally distinguishable in the halo bias. We propose here a generalization of the local ansatz that is phenomenologically useful and captures the physics of many possible multi-field models. The generalized ansatz allows for different types of scale-dependent amplitude $f_{\rm NL}$ along with the standard local shape.

While signatures of primordial non-Gaussianity in LSS can often be predicted analytically, accurate comparisons of observables with theoretical predictions require the intermediate step of numerical simulations to validate or correct any proposed analytical relations. In this paper we build on previous work of Dalal et al. [15] to numerically investigate the effect of scale-dependent, local non-Gaussian initial conditions. Interestingly, we find theoretically and numerically that the halo bias is sensitive to two different types of scale dependence that can constrain and distinguish between inflationary models. However unlike in the constant $f_{\rm NL}$ case, the simplest theoretical prediction for the bias in models with scale-dependent non-Gaussianity does not fully agree with our numerical results. In this paper we will motivate our new non-Gaussian ansatz, present the analytic predictions from that model and the associated simulations. We will discuss a possible explanation for the discrepancy, which indicates that this problem constitutes an interesting test for our understanding of structure growth, although we postpone a detailed analysis for future work.

The paper is organized as follows. In section 2 we discuss in more detail the motivation from inflationary theory. A self-contained and purely phenomenological discussion starts in section 3, where we use the peak-background split method to demonstrate the qualitative ways scale-dependent non-Gaussianity may be observable. We also present forecasts for differentiating the bispectra based on the analytic predictions. In section 4 we show the results of numerical simulations, which demonstrate a stronger signal than the analytic prediction, and so are encouraging for the observational prospects. We speculate on a possible explanation for the discrepancy between theory and simulation and then conclude in section 5.

2 A bigger family for the local ansatz

The original "local ansatz" to add non-Gaussianity to the primordial perturbations is [20–22]:

$$\Phi(\mathbf{x}) = \Phi_G(\mathbf{x}) + f_{\rm NL}\left[\Phi_G^2(\mathbf{x}) - \langle\Phi_G^2(\mathbf{x})\rangle\right] + \ldots, \tag{2.1}$$

JCAP03(2011)017

where $\Phi(\mathbf{x})$ is (minus) the gravitational potential, $\Phi_G(\mathbf{x})$ is a Gaussian random field and the degree of non-Gaussianity is parameterized by (typically constant) $f_{\rm NL}$. Here a positive $f_{\rm NL}$ leads to a positive skewness in the density perturbations, and so more very large objects, in the same sign convention as WMAP [23].[1]

In many scenarios the primary effect of the non-Gaussian correction appears as a non-zero bispectrum, defined as

$$\langle \Phi(\boldsymbol{k}_1)\Phi(\boldsymbol{k}_2)\Phi(\boldsymbol{k}_3)\rangle \equiv (2\pi)^3\,\delta_D^3(\boldsymbol{k}_1+\boldsymbol{k}_2+\boldsymbol{k}_3)B_\Phi(\boldsymbol{k}_1,\boldsymbol{k}_2,\boldsymbol{k}_3)\,. \tag{2.2}$$

For the local ansatz above the bispectrum is

$$B_\Phi(\boldsymbol{k}_1,\boldsymbol{k}_2,\boldsymbol{k}_3) \;=\; f_{\rm NL}\,[2\,P_\Phi(\boldsymbol{k}_1)P_\Phi(\boldsymbol{k}_2)+2\,\text{perm.}]\,, \tag{2.3}$$

where as usual we define

$$\langle \Phi(\boldsymbol{k}_1)\Phi(\boldsymbol{k}_2)\rangle \equiv (2\pi)^3\,\delta_D^3(\boldsymbol{k}_1+\boldsymbol{k}_2)P_\Phi(k_1) = (2\pi)^3\,\delta_D^3(\boldsymbol{k}_1+\boldsymbol{k}_2)\frac{2\pi^2\Delta_\Phi^2(k_1)}{k_1^3}. \tag{2.4}$$

The subscript D distinguishes the Dirac delta function from the density perturbation. Assuming the spectral index, n_s, has no significant k-dependence, the dimensionless power spectrum is given by $\Delta_\Phi^2 = A_0(k/k_0)^{n_s-1}$.

CMB data (WMAP7) already constrain $-10 < f_{\rm NL} < 74$ at 95% confidence ([26]; see also [27, 28]) and could potentially achieve $\Delta f_{\rm NL} \sim$ few from the Planck satellite [23, 29–31]. The best current constraint from LSS comes from the scale-dependent bias induced in the galaxy power spectrum, giving $-29 < f_{\rm NL} < 69$ at 95% CL ([17]; see also [18, 32]).

While the local ansatz is a useful phenomenological tool, it is only a first step toward modeling and constraining primordial non-Gaussianity motivated by the fundamental physics of inflation. Specifically, the local ansatz resembles the first term in a series that arises from the transfer of isocurvature to curvature fluctuations during or at the end of inflation. Such a transfer may be due to additional scalar fields during inflation (multi-field [33–47]), or after (the curvaton scenario [45, 48–55]), or inhomogeneous reheating [56, 57].

There are at least four possible sources of non-Gaussianity that generate bispectra that are largely well-captured by the local ansatz shape in the final curvature perturbations. First, a spectator field during inflation is not constrained to have a flat potential, so there may be intrinsic non-Gaussianity in that field that is not tightly constrained by the slow-roll conditions and which can be transferred to non-Gaussianity in the curvature. Second, in multi-field models non-linear evolution of curvature modes outside the horizon will generate non-Gaussianity in the observed curvature perturbations even if the field(s) themselves have no interactions other than gravitational [45]. Third, the conversion of curvaton isocurvature fluctuations to curvature after inflation depends on the energy density in the curvaton field, which is at least quadratic in the fluctuations and so introduces non-Gaussianity of the local type [48]. Finally, loop corrections may, in special cases, generate a scale-dependent non-Gaussianity [58].

[1] We use the convention that $f_{\rm NL}$ is defined in terms of (minus) the gravitational potential early in the matter era. We caution that there is another convention (used, for example, in [24, 25]) that defines $f_{\rm NL}^{\rm LSS}$ in terms of the gravitational potential normalized to present day amplitude, which is related to the WMAP convention used here by $f_{\rm NL}^{\rm LSS} = f_{\rm NL}(g(z=\infty)/g(z=0))$ ($\approx 1.36 f_{\rm NL}$ in the WMAP7 cosmology), where $g(z=0)/g(\infty)$ is often referred to as the growth suppression factor.

JCAP03(2011)017

Phenomenologically, we can write a more general ansatz for the bispectrum of (minus) the gravitational potential that is factorizable and symmetric in momentum by introducing two functions, $\xi_s(k)$ and $\xi_m(k)$:

$$B_\Phi(\boldsymbol{k}_1, \boldsymbol{k}_2, \boldsymbol{k}_3) = \xi_s(k_3)\xi_m(k_1)\xi_m(k_2)P_\Phi(k_1)P_\Phi(k_2) + 5 \text{ perm} . \tag{2.5}$$

This ansatz captures a wide range of physically motivated and perturbatively controlled models, where the functions $\xi_{s,m}$ are at most weak functions of scale. The notation refers to the physical origin of the two functions in inflationary scenarios: ξ_s, with s for single field, is different from one if one of the fields has non-trivial self interactions or nonlinearly sources curvature perturbations; ξ_m, with m for multi-field, is different from one when two or more fields both contribute to the power in curvature fluctuations. We will discuss several illustrative examples next.

2.1 Two field inflation

First, we consider a two field inflation scenario where running non-Gaussianity can be obtained, following [35, 44]. In the δN formalism [59, 60], one uses the dependence on the number of e-folds of inflation on the fields present to relate the curvature fluctuations to the scalar field fluctuations. Even if a field does not source the inflationary Hubble parameter H, the point where inflation ends (and so the number of e-folds, N) can still depend on the position of the field. Then, we can express the curvature perturbation resulting from fluctuations of two fields ϕ and σ (up to second order) as

$$\zeta(k) = N_{,\phi}(k)\delta\phi(k) + N_{,\sigma}(k)\delta\sigma(k) + \frac{1}{2}N_{,\sigma\sigma}(k)[\delta\sigma \star \delta\sigma](k) \ + \ldots \tag{2.6}$$

where for simplicity we have assumed one of the non-Gaussian terms ($N_{,\sigma\sigma}$) dominates the other ($N_{,\phi\phi}$) and $N_{,\phi\sigma} = 0$. All quantities are evaluated at horizon crossing for the mode k, and $N_{,\phi}$ is the derivative of the number of e-folds with respect to the field ϕ. To gain some intuition about the pattern of multiplications and convolutions in this expression, recall that in single field inflation the running of $N_{,\phi} = -\frac{H}{\dot\phi} \sim 1/\sqrt{\epsilon}$ contributes the term proportional to the second slow-roll parameter ($\eta = \frac{\dot\epsilon}{H\epsilon}$) in the spectral index. In addition, the form of the quadratic term generates the standard result that the bispectrum in the squeezed limit goes like the spectral index, $n_s - 1$, evaluated at horizon crossing of the short wavelength (large k) modes [61] (although one must take into account pre-horizon crossing non-Gaussianity generated in the statistics of the field $\delta\phi$ to get the complete bispectrum correct). In the single field case, the amplitude of the non-Gaussianity in the curvature perturbation is small, but it does run if the spectral index runs and the dominant term has scale-dependent $f_{\rm NL}$ evaluated at the scale of the short modes.[2]

In a multi-field scenario, the modes for each individual field have fluctuations of order H, so that

$$\begin{aligned}\left\langle \delta\phi(\mathbf{k})\delta\phi(\mathbf{k}')\right\rangle = \left\langle \delta\sigma(\mathbf{k})\delta\sigma(\mathbf{k}')\right\rangle &= (2\pi)^3\delta_D^3(\mathbf{k}+\mathbf{k}')\frac{(2\pi^2)}{k^3}\frac{H_*^2}{4\pi^2} \\ &\equiv (2\pi)^3\delta_D^3(\mathbf{k}+\mathbf{k}')P(k) .\end{aligned} \tag{2.7}$$

[2] A detailed discussion of how this is consistent with real-space formulations of the local ansatz can be found in [62].

JCAP03(2011)017

where the asterisk is a reminder that H is evaluated at horizon-crossing for each wavenumber k. Then the total curvature power spectrum can be written

$$\begin{aligned}\left\langle\zeta(\mathbf{k})\zeta(\mathbf{k}')\right\rangle &\equiv (2\pi)^3\delta_D^3(\mathbf{k}+\mathbf{k}')P_\zeta(k) \\ &= (2\pi)^3\delta_D^3(\mathbf{k}+\mathbf{k}')P(k)(N_{,\phi}^2+N_{,\sigma}^2) \\ &= (2\pi)^3\delta_D^3(\mathbf{k}+\mathbf{k}')[P_{\zeta(\phi)}+P_{\zeta(\sigma)}]\,.\end{aligned} \tag{2.8}$$

The tree-level bispectrum, assuming $\langle\delta\phi\delta\sigma\rangle = 0$, is

$$\begin{aligned}B_\zeta(\mathbf{k}_1,\mathbf{k}_2,\mathbf{k}_3) &= \frac{1}{2}N_{,\sigma\sigma}(k_3)\,\frac{P_{\zeta(\sigma)}(k_1)}{P_\zeta(k_1)}\frac{P_{\zeta(\sigma)}(k_2)}{P_\zeta(k_2)}\,P_\zeta(k_1)P_\zeta(k_2) + 5\,\text{perm.}, \\ B_\Phi(\mathbf{k}_1,\mathbf{k}_2,\mathbf{k}_3) &\equiv \xi_s(k_3)\xi_m(k_1)\xi_m(k_2)\,P_\Phi(k_1)P_\Phi(k_2) + 5\,\text{perm.},\end{aligned} \tag{2.9}$$

where $N_{,\sigma\sigma}$ depends on non-trivial self (and gravitational) interaction terms of just the field σ, so we relabel it ξ_s, with s for single field. The fraction of power in the σ field is different from one only if both fields contribute significantly to the power in fluctuations so we have labeled this function with an m for multi-field. (Otherwise, the bispectrum would reduce to the usual single-field expression, where $f_{\rm NL}$ must be of order slow-roll - that is, the term quadratic in $\delta\phi$ would be most important, giving a bispectrum with the same form as the first line of eq. (2.9) but with the coefficient of the power spectrum terms $N_{\phi\phi}(k)$.) Assuming that the potential Φ is defined in the matter era, the precise relationship between the first and second lines above is

$$\begin{aligned}\frac{5}{6}N_{,\sigma\sigma}(k) &= \xi_s(k) \\ \frac{P_{\zeta(\sigma)}(k)}{P_\zeta(k)} &= \xi_m(k)\,.\end{aligned} \tag{2.10}$$

We note that quite generally all the coefficients $N_{,\phi}$, $N_{,\sigma}$, $N_{,\sigma\sigma}$, etc will be scale-dependent as the potentials for the fields are not exactly flat. In that sense, in any two-field scenario with large local non-Gaussianity, running of the amplitude through the function $\xi_s(k)$ is as natural as running of the spectral index. It may be somewhat fine-tuned to have two fields contribute to the amplitude of fluctuations (although this is hard to say in the absence of compelling particle physics realizations of inflation), but if they do it is likely natural for their potentials to be slightly different so that $\xi_m(k_2)$ is scale-dependent. We will parametrize this scale dependence by writing

$$\xi_{s,m}(k) = \xi_{s,m}(k_p)\left(\frac{k}{k_p}\right)^{n_f^{(s),(m)}} \tag{2.11}$$

where k_p is a (theoretically irrelevant) pivot point.

2.2 Mixed curvaton/inflaton scenario

Now suppose the curvature perturbation comes partly from a Gaussian inflaton field (ϕ) and partly from a 'curvaton' field (σ) which was a spectator during inflation but contributes to the curvature perturbation afterwards [48, 63–67]. The curvaton naturally has a contribution

JCAP03(2011)017

that is quadratic in real space since it contributes proportionally to the energy density in its fluctuations. Assuming a purely quadratic potential for the curvaton gives

$$\rho_\sigma = \frac{1}{2}m_\sigma^2(\sigma+\delta\sigma)^2 \Rightarrow \delta\rho_\sigma = \frac{1}{2}m^2(2\sigma\delta\sigma+\delta\sigma^2). \tag{2.12}$$

The field fluctuations are still generated during inflation, with amplitude $\sqrt{\langle\delta\sigma^2\rangle} = H/2\pi$. The quadratic term means that the curvaton can contribute a local-type non-Gaussianity with $f_{\rm NL}$ constant and determined by the proportion of energy in the curvaton at the time the field decays.

Then we can write the total curvature field as a sum of contributions from the inflaton and curvaton:

$$\zeta(x) = \zeta_\phi(x) + \zeta_\sigma(x) + \frac{3}{5}f_{\rm NL}^\sigma(\zeta_\sigma(x)^2 - \langle\zeta_\sigma(x)^2\rangle) \tag{2.13}$$

where the factor of 3/5 enters since $f_{\rm NL}$ is conventionally defined for the matter era potential (eq. (2.1)) rather than the primordial curvature.

Assuming the fields don't couple, the bispectrum takes the familiar local form, but now in terms of $P_{\zeta(\sigma)}$:

$$B_\zeta(\boldsymbol{k}_1,\boldsymbol{k}_2,\boldsymbol{k}_3) = \frac{3}{5}f_{\rm NL}^\sigma[P_{\zeta(\sigma)}(k_1)P_{\zeta(\sigma)}(k_2) + 5\,\text{sym}]\ . \tag{2.14}$$

If we define the ratio of power contributed by the curvaton

$$\xi(k) = \frac{P_{\zeta(\sigma)}(k)}{P_{\zeta(\sigma)}(k)+P_{\zeta(\phi)}(k)} = \frac{P_{\zeta(\sigma)}(k)}{P_\zeta(k)} \tag{2.15}$$

we can write

$$\begin{aligned} B_\zeta(\boldsymbol{k}_1,\boldsymbol{k}_2,\boldsymbol{k}_3) &= \frac{3}{5}f_{\rm NL}^\sigma[\xi(k_1)\xi(k_2)P_\zeta(k_1)P_\zeta(k_2) + 5\,\text{perm}] \\ B_\Phi(\boldsymbol{k}_1,\boldsymbol{k}_2,\boldsymbol{k}_3) &\equiv \xi_m(k_1)\xi_m(k_2)P_\Phi(k_1)P_\Phi(k_2) + 5\,\text{perm} \end{aligned} \tag{2.16}$$

where we have absorbed $f_{\rm NL}^\sigma$ into ξ_m, that is $\xi_m(k) = \sqrt{f_{\rm NL}^\sigma}\xi(k)$. Again, we parametrize the function $\xi_m(k)$ as a simple power law, $\xi_m(k) \propto k^{n_f^{(m)}}$.

2.3 Curvaton alone

If non-Gaussianity comes from the curvaton alone, and a potential other than quadratic is considered, the bispectrum can again take the form [68, 69]

$$B_\Phi(\mathbf{k}_1,\mathbf{k}_2,\mathbf{k}_3) \equiv \xi_s(k_3)P_\Phi(k_1)P_\Phi(k_2) + 5\,\text{perm.}, \tag{2.17}$$

where $\xi_s(k)$ can be parametrized as a power law, at least for some potentials, and $n_f^{(s)}$ apparently can have either sign. Inhomogeneous reheating may similarly generate this bispectrum [62].

JCAP03(2011)017

2.4 Relation to the spectral index

The running of $\xi_m(k)$ is an important physical feature of either type of two-field model: it is the evolution of the relative power in the two fields during inflation. Just as the spectral index measures the variation of the overall amplitude of fluctuations during inflation, for two-field models the bispectral index $n_f^{(m)}$ can provide complementary information about how the contribution from each field evolves. For some curvaton scenarios there would be a link between running non-Gaussianity and large scale power asymmetry in the CMB [70].

There is a precise relationship between the spectral index and the bispectral index $n_f^{(m)}$:

$$\begin{aligned} \frac{d\ln P_\zeta}{d\ln k} &\equiv n_s - 1 \\ \frac{d\ln P_{\zeta(\sigma)}}{d\ln k} &\equiv n_\sigma - 1 \\ \frac{d\ln \xi_m}{d\ln k} &\equiv n_f^{(m)} = n_\sigma - n_s \end{aligned} \tag{2.18}$$

Although the running of the bispectrum may have either sign, models with a red tilt for the field σ are anecdotally more common and in that case we have

$$n_f^{(m)} \leq -(n_s - 1)\ . \tag{2.19}$$

Notice that some of the literature (e.g. [45]) defines $f_{\rm NL}(k) = \xi_m(k)^2$ and so quotes $n_f \leq -2(n_s-1)$. Here however, we will see that there are two different shifts in the non-Gaussian bias, each dependent on one factor of $\xi_m(k)$, so we define $n_f^{(m)}$ as the running in that function. Finally, notice that the spectral index of the observed curvature perturbation depends on the running of both fields ϕ and σ. If the running of the fields is large enough, it will change which field dominates the curvature statistics.

Whatever the origin of the running in either function $\xi_{m,s}$, it parametrizes the deviation from exactly quadratic potentials in either field and so is expected to be generically on the order of slow-roll parameters (and should be to avoid substantial corrections to this parameterization). We will use somewhat large values of the running to confirm the behavior of this type of model in our simulations, but the observational goal should be to measure $|n_f^{(s),(m)}| \sim \mathcal{O}(n_s - 1)$. We discuss the potential of future surveys to reach this goal in section 5. For the standard quadratic curvaton case, $n_f^m > 0$ seems more natural (that is, non-Gaussianity increases on small scales) while Byrnes et al. [44] found $0 > n_f^{(s)} \gtrsim -0.1$ in a survey of multi-field hybrid inflation models. The sign can be understood if the non-Gaussianity is entirely due to non-linear evolution outside the horizon. Then large scale modes (which exit earlier) will to be more non-Gaussian than small scale modes.[3,4]

[3]Previous authors have employed different notation for scale-dependent local models. In particular, Byrnes et al, in an extensive discussion of possible multi-field bispectra [62] propose a definition of $f_{\rm NL}$ and its running that for our ansatz correspond to $f_{\rm NL}^{\rm Byrnes}(k_1,k_2,k_3) \equiv [\xi_s(k_3)\xi_m(k_1)\xi_m(k_2)P_\Phi(k_1)P_\Phi(k_2) + {\rm sym}]/[P_\Phi(k_1)P_\Phi(k_2) + {\rm sym}]$ and $n_{f_{\rm NL}}^{\rm Byrnes} \equiv d\ln|f_{\rm NL}^{\rm Byrnes}(k_1=k_2=k_3=k)|\,/\,d\ln k = n_f^{(s)} + 2n_f^{(m)}$.

[4]In a discussion of the ability of observations to constrain two-field models of the mixed curvaton/inflaton type, Tseliakhovich et al [71] recently defined a variable x_1 where $x_1 = \xi_m^2$ and where only the scale-independent case was considered. In addition, their function ξ is defined differently: $\xi^{\rm here} = 1/(1+(\xi^{\rm there})^2)$.

JCAP03(2011)017

2.5 A comment on naturalness and completeness

Given that it is already difficult to convincingly explain one field with a very flat potential, we may reasonably ask if the scenarios we are considering are even less likely than the usual single-field inflation. It is very hard to answer that question without better fundamental models - it may be that where there is one inflaton-like field, there are naturally several (especially in higher dimensional models), or not. In inflation, there is a very compelling reason why the spectral index should be slightly different from one: old inflation models with exact de Sitter space are difficult to connect to the early, hot universe after inflation, while slow-roll with the Hubble parameter not exactly constant can have a natural end to inflation and a period of reheating. *If* the slow-roll scenario is right and *if* two fields are present and relevant during inflation, it may be reasonable to expect that they both have nearly flat and yet not identical potentials. If one accepts that local type non-Gaussianity is natural (or more compellingly, if it is observed), scale dependence is also natural. In the absence of a range of compelling high energy models, it is hard to quantify the likelihood of any of these scenarios.

However, from a phenomenological point of view, considering a generalized local ansatz is helpful in two ways: first, it argues for a careful analysis of different mass tracers in any test for primordial local type non-Gaussianity and second, it provides a test of our understanding of structure formation. As we will see, the existing expressions for halo bias do not give particularly satisfactory agreement with our simulations.

The generalized local ansatz above is useful to uncover new observational signatures, and it would be interesting to investigate to what extent it holds in more complicated models with more (and coupled) fields. However, even with this ansatz we are still far from considering all possible known effects. In most two field models, we expect higher order terms (like a ζ^3 contribution) to be present in the expression for the non-Gaussian curvature. Those corrections are also important for comparison of observation with realistic models and have been considered in [52, 72–76]. In addition, there are other possibilities that require something even more general than the symmetric, factorizable form. For example, non-gaussianity generated by loop effects can sometimes be large and goes like [58]

$$\langle\zeta^3\rangle \propto f_{\rm NL}(\min\{k_1,k_2,k_3\})[P(k_1)P(k_2)+5\,\text{perm.}] \tag{2.20}$$

In addition, the power-law behavior of our ansatz is a poor model for scenarios with a feature at some particular scale, such as [77] (features in the potential) or [78] where non-Gaussianity effectively switches on at some scale where a spectator field becomes light.

Finally, we note that scale-dependent non-Gaussianity may also arise in other ways and for other bispectra, but most other examples in standard inflationary models are less divergent in the squeezed limit than the local shape is and so have a weaker signal in the bias. However, there is a small region of parameter space in ekpyrotic models that seems to generate bispectra with scale-dependent amplitudes consistent with current observations, and *more* divergent than the local ansatz [79].

3 Generalized local ansatz and large scale structure statistics

Our ansatz for the factorizable, symmetric, scale-dependent local bispectrum is

$$B_\Phi(\boldsymbol{k}_1,\boldsymbol{k}_2,\boldsymbol{k}_3) = \xi_s(k_3)\xi_m(k_1)\xi_m(k_2)P_\Phi(k_1)P_\Phi(k_2) + 5\,\text{perm}\,. \tag{3.1}$$

JCAP03(2011)017

where we parametrize the k-dependence of the amplitude as

$$\xi_{s,m}(k) = \xi_{s,m}(k_p)\left(\frac{k}{k_p}\right)^{n_f^{(s),(m)}} \quad . \tag{3.2}$$

with $|n_f^{(s),(m)}| < 1$. Ideally, the pivot scale k_p can be chosen at a point where the amplitude and running of the shape are as close to uncorrelated as possible. We adopt $k_p = 0.04\,\mathrm{Mpc}^{-1}$ based on analysis for the CMB in [80], although they used a slightly different ansatz for the scale dependence. Note, however, that the constraints on $\xi_{s,m}(k)$ will be entirely independent of the chosen value of k_p.

Although generically we might expect both functions $\xi_s(k)$ and $\xi_m(k)$ to be present, we can consider the two functions separately for simplicity. For that reason, we will compare the following two bispectra in what follows:

$$\begin{aligned} B^s_\Phi(\boldsymbol{k}_1, \boldsymbol{k}_2, \boldsymbol{k}_3) &= \xi_s(k_1) P_\Phi(k_2) P_\Phi(k_3) + 5\,\mathrm{perm} \\ B^m_\Phi(\boldsymbol{k}_1, \boldsymbol{k}_2, \boldsymbol{k}_3) &= \xi_m(k_1)\xi_m(k_2) P_\Phi(k_1) P_\Phi(k_2) + 5\,\mathrm{perm} \end{aligned} \tag{3.3}$$

The first line applies to a model where only one field contributes to the curvature perturbations (and the inflationary background is sourced by something else). For example, it is generated by a curvaton model where the potential has terms other than the mass term, eq. (2.17), or from a simplified version of the δN case from section 2 (where we take $\xi(k)$, the ratio of power in the two fields, to be constant). Since the curvature perturbations come only from one field, we label the new function $\xi_s(k)$ with s for single field. Scale-dependence in this function indicates the presence of non-trivial self-interactions (eg, deviation of the curvaton potential from exactly quadratic). The second line corresponds to a scenario where (at least) two fields contribute to the curvature perturbations, but the relevant self-interactions are purely quadratic. For example, this is the mixed inflaton/curvaton model of eq. (2.16), where the curvaton has only a quadratic potential. The label m on $\xi_m(k)$ indicates that multiple fields contribute to the curvature perturbations. Scale-dependence in ξ_m shows how much the potentials for the fields differ.

Notice that the first model in eq. (3.3) has a form that is equivalent to the bispectrum one would get from generalizing the local ansatz by

$$\Phi(\mathbf{x}) = \Phi_G(\mathbf{x}) + f_{\mathrm{NL}} * \left[\Phi_G^2(\mathbf{x}) - \langle \Phi_G^2(\mathbf{x})\rangle\right] \ . \tag{3.4}$$

This also justifies the single-field label. Scale dependence of this type was studied recently in ref. [81].

3.1 Scale-independent non-Gaussianity and bias

In this section we will work out a prediction for the possible signatures of our generalized local ansatz in the halo power spectrum. We will only be concerned with the behavior of the power spectrum at very small k, where the deviation from the Gaussian case is largest. The matter perturbations δ at redshift z are related to the perturbations in the early matter era potential Φ by

$$\begin{aligned} \delta(\vec{k}, z) &= M(k, z)\Phi(\vec{k}) \\ M(k, z) &= \frac{2}{3}\frac{1}{\Omega_m}\frac{c^2}{H_0^2} D(z)\frac{g(0)}{g(\infty)} T(k) k^2, \end{aligned} \tag{3.5}$$

JCAP03(2011)017

so that $P_\delta(k,z) = M^2(k,z)P_\Phi(k)$. Here Ω_M is the matter density relative to critical, H_0 is the Hubble constant, $D(z)$ is the linear growth function at redshift z normalized to one today, and the growth suppression factor is $\frac{g(z=0)}{g(z=\infty)} \simeq 0.76$ in the best-fit ΛCDM model. We use the Eisenstein & Hu [82] fit to the transfer function $T(k)$. The variance of density fluctuations at redshift z smoothed on a scale R associated to mass M is $\sigma^2(M,z)$, defined by

$$\sigma^2(M,z) = \int_0^\infty \frac{dk}{k} W_R(k)^2 M(k,z)^2 \Delta^2_\Phi(k). \tag{3.6}$$

where the power spectrum of the primordial curvature perturbations is given by eq. (2.4) and $W_R(k)$ is the Fourier transform of the top-hat window function. The spatial smoothing scale R is related to the smoothing mass scale M via

$$M = \frac{4}{3}\pi R^3 \rho_{m,0}, \tag{3.7}$$

where $\rho_{m,0}$ is the matter energy density today. We write the combination $M(k,z)W_R(k) \equiv M_R(k,z)$.

3.2 Peak-background split and halo bias

Halos in N-body simulations are associated with peaks of the initial, linear density field $\delta \propto k^2\Phi$, whose heights exceed some threshold [83, 84]. The basic idea of the peak-background split [85] is to compute the effect of long-wavelength background modes on the heights of small-scale peaks, and thereby estimate the large-scale clustering of halos. The procedure used in the peak-background split is to perturb a single background mode $\Delta\Phi(\boldsymbol{k}_l)$ and propagate the effect of this perturbation to the height of a peak near threshold. In Gaussian cosmologies, where there is no mode coupling, the heights of peaks are simply boosted by the density associated with the background mode, $\Delta\delta(\boldsymbol{k}_l) \propto k_l^2 \Delta\Phi(\boldsymbol{k}_l)$. With non-Gaussianity, however, there is mode coupling, so we have to compute how this background mode affects shorter-wavelength modes $\Phi(\boldsymbol{k}_s)$ as well. This clearly involves looking at the bispectrum in the *squeezed* limit $B_\Phi(\boldsymbol{k}_l, \boldsymbol{k}_s, -\boldsymbol{k}_s - \boldsymbol{k}_l \approx -\boldsymbol{k}_s)$ where $k_l \ll k_s$.

Using the argument above, we can predict the consequences of modifying the local ansatz to include some form of scale dependence; our discussion here is similar to that in [86–88]. To get a feel for the effect of the scale-dependent non-Gaussianity on the bias, notice that we can rewrite the expression for the ΔN type non-Gaussian field (the first line of eq. (3.3)) in Fourier space as a sum of Gaussian modes $\Phi_G(k)$ and a non-Gaussian piece $\Phi_B(k)$ designed to recover the single-field model bispectrum:

$$\begin{aligned} \Phi(\mathbf{k}) &= \Phi_G(\mathbf{k}) + \Phi_B(\mathbf{k}) \\ \Phi_B(\mathbf{k}) &= \xi_s(k) \int \frac{d^3q_1}{(2\pi)^3} \int \frac{d^3q_2}{(2\pi)^3} \delta^3_D(\mathbf{q}_1 + \mathbf{q}_2 + \mathbf{k}) \Phi(\mathbf{q}_1)\Phi(\mathbf{q}_2) \end{aligned} \tag{3.8}$$

where we have dropped the $\delta^3_D(\mathbf{k})$ term which is not important for this discussion. Now we can use eq. (3.8) to consider the effect of some long-wavelength perturbation $\Delta\Phi(\boldsymbol{k}_l)$. Considering $\boldsymbol{k} \approx -\mathbf{q}_2 \approx \boldsymbol{k}_s$ and $\mathbf{q}_1 = \boldsymbol{k}_l$ in that expression we see that

$$\Delta\Phi_B(\boldsymbol{k}_s) = 2\xi_s(\boldsymbol{k}_s)\Delta\Phi(\boldsymbol{k}_l)\Phi(\boldsymbol{k}_s) \tag{3.9}$$

$$\Delta\delta(\boldsymbol{k}_s) = 2\xi_s(\boldsymbol{k}_s)\Delta\Phi(\boldsymbol{k}_l)\delta(\boldsymbol{k}_s) \tag{3.10}$$

JCAP03(2011)017

where in the latter equation, we have used the Poisson equation. We then sum over all the short wavelengths to get the total boost in peak height, which then translates into the halo excess and halo bias.

To see how this works, let us compute the effect of non-Gaussianity on a typical peak. Consider a peak of the smoothed density field,

$$\delta_R(\boldsymbol{x}) = \int \frac{d^3\boldsymbol{k}}{(2\pi)^3}\delta(\boldsymbol{k})W(kR)e^{-i\boldsymbol{k}\cdot\boldsymbol{x}} \tag{3.11}$$

whose height is $\delta_{\rm pk} = \nu\sigma$, where σ is given by eq. (3.6). The average density profile around such a peak was first determined by Bardeen et al. [89]. Below in section 3.3 we assume the limit $\nu \gg 1$, and if we adopt the same limit here, this average profile is given by

$$\langle\delta(r)|\delta_{\rm pk}\rangle = \frac{\xi_{us}(r)}{\sigma^2}\delta_{\rm pk}, \tag{3.12}$$

where again σ^2 is given by eq. (3.6), and

$$\xi_{us}(r) = \int \frac{k^2dk}{2\pi^2}P_\delta(k)W(kR)j_0(kr) \tag{3.13}$$

is the cross-correlation function between the unsmoothed density δ and the smoothed density δ_R, at separation r. For any finite ν, there is also a term in the average profile proportional to $\nabla^2\xi$ that steepens the profile [89] and that is easy to include, but we omit it here for clarity.

Our expression in eq. (3.10) requires the peak profile in $\boldsymbol{k}$-space, so we Fourier transform eq. (3.13), which gives

$$\delta(\boldsymbol{k}) = \frac{\delta_{\rm pk}}{\sigma^2}P_\delta(k)W(kR). \tag{3.14}$$

Inserting this expression into eq. (3.10) gives the change in the $\boldsymbol{k}$-space peak profile, which we then smooth and Fourier transform to obtain the total boost in the smoothed peak height:

$$\begin{aligned}\Delta\delta_{\rm pk} &= \int \frac{k^2dk}{2\pi^2}W(kR)\Delta\delta(k)\\ &= 2\Delta\Phi\frac{\delta_{\rm pk}}{\sigma^2}\int \frac{k^2dk}{2\pi^2}P_\delta(k)W^2(kR)\xi_s(k).\end{aligned} \tag{3.15}$$

For scale-independent non-Gaussianity, where $\xi_s(k) = f_{\rm NL}$, this expression reduces to the familiar $\Delta\delta_{\rm pk} = 2f_{\rm NL}\Delta\Phi\delta_{\rm pk}$ [15]. For the more general case of scale-dependent non-Gaussianity, $f_{\rm NL}$ is replaced by an *effective* coefficient

$$f_{\rm NL}^{\rm eff} = \sigma^{-2}\int \frac{k^2dk}{2\pi^2}P_\delta(k)W^2(kR)\xi_s(k) = \sigma^{-2}\int \frac{k^2dk}{2\pi^2}P_\Phi(k)M_R^2(k)\xi_s(k). \tag{3.16}$$

We see that the presence of the scale-dependent function $\xi_s(k)$ implies that collapsed objects have a shift in bias with amplitude given by an effective $f_{\rm NL}$ roughly on the scale of the object. That is, if $\xi_s(k)$ (which in this simple case is like $f_{\rm NL}(k)$ as in eq. (3.4)) increases on small scales, smaller mass objects will have a larger non-Gaussian correction than very massive objects.

JCAP03(2011)017

For the curvaton type model, the second line of eq. (3.3), the effect above comes along with an additional k-dependence in the bias:

$$\Delta\delta(\boldsymbol{k}_s) = 2\xi_m(\boldsymbol{k}_l)\xi_m(\boldsymbol{k}_s)\Delta\Phi(\boldsymbol{k}_l)\delta(\boldsymbol{k}_s). \tag{3.17}$$

In this case, different mass tracers have a non-Gaussian shift in bias, Δb, with an amplitude proportional to an "effective $f_{\rm NL}$" set by their mass (a consequence of $\xi_m(\mathbf{k}_s)$) *and* a scale dependence that goes as $k^{-(2-n_f)}$ (a consequence of $\xi_m(\mathbf{k}_l)$).

On a final note, recall that we have taken the high-peak limit $\nu \to \infty$, in which the average peak profile is simply proportional to the matter correlation function $\xi_{us}(r)$. More realistically, the typical peak profile for the relevant regime $\nu \sim 1$ is considerably steeper than this. This change in the peak profile is irrelevant for scale-independent non-Gaussianity, but it can be important for scale-dependent non-Gaussianity, since the peak profile in Fourier space can extend to much higher k than implied by eq. (3.14). This can change the mass dependence of $f_{\rm NL}^{\rm eff}$, a point that we will return to in section 4.

3.3 Alternative derivation of scale-dependent effects

The intuitive procedure above leads to essentially the same result as the procedure outlined by Grinstein and Wise [90] and further developed by Matarrese et al. [91]. For a generic non-Gaussian distribution, refs. [90, 91] found a way to express the two-point function of peaks in terms of a series expansion in correlation functions; this expansion is valid in the high-peak limit ($\nu \gg 1$, where ν is defined just below). Motivated by the results of [15], this expression was recently applied to the case of local non-Gaussianity by Matarrese and Verde [92]. We can use the same starting point to consider the effects of our generalized local ansatz, and express the two-point function for halos of mass M ($\xi_{h,M}(|\vec{x}_1 - \vec{x}_2|)$) in terms of the n-point functions of the density field smoothed on the associated scale R ($\xi_R^{(n)}(\vec{x}_1, \ldots, \vec{x}_n)$)

$$\xi_{h,M}(|\vec{x}_1 - \vec{x}_2|) = \frac{\nu^2}{\sigma(M)^2}\xi_R^{(2)}(\vec{x}_1, \vec{x}_2) + \frac{\nu^3}{2\sigma(M)^3}[\xi_R^{(3)}(\vec{x}_1, \vec{x}_1, \vec{x}_2) + \xi_R^{(3)}(\vec{x}_1, \vec{x}_2, \vec{x}_2)] + \ldots \tag{3.18}$$

where the dots represent higher order terms (both higher correlation functions and higher powers of the two- and three-point function). The collapse threshold δ_c is contained in $\nu \equiv \delta_c/\sigma(M)$. Now we can use the Fourier transform of the halo auto-correlation, eq. (3.18), to compute the bias:

$$\begin{aligned} P_{M,h}(k,z) = {} & \frac{\nu^2(z)}{\sigma(M,z)^2}P_{\delta,R}(k,z) + \frac{\nu^3(z)}{2\pi^2\sigma(M,z)^3}P_\Phi(k)M_R(k,z) \\ & \times\xi_s(k_p)[\xi_m(k_p)]^2\left(\frac{k}{k_p}\right)^{n_f^{(m)}}\int_0^\infty dk_1\, k_1^2 P_\Phi(k_1)M_R(k_1,z)\int_{-1}^1 d\mu\, M_R(\tilde{k},z) \\ & \times\left[\frac{P_\Phi(\tilde{k})}{P_\Phi(k)}\left(\frac{k_1\tilde{k}}{k_p^2}\right)^{n_f^{(m)}}\left(\frac{k}{k_p}\right)^{n_f^{(s)}-n_f^{(m)}} + \left(\frac{\tilde{k}}{k_p}\right)^{n_f^{(s)}}\left(\frac{k_1}{k_p}\right)^{n_f^{(m)}} + \frac{P_\Phi(\tilde{k})}{P_\Phi(k_1)}\left(\frac{k_1}{k_p}\right)^{n_f^{(s)}}\left(\frac{\tilde{k}}{k_p}\right)^{n_f^{(m)}}\right] \\ = {} & \frac{\nu^2(z)}{\sigma(M,z)^2}P_{\delta,R}(k,z)\left[1 + \frac{4\delta_c}{M_R(k,z)}\xi_s(k_p)[\xi_m(k_p)]^2\left(\frac{k}{k_p}\right)^{n_f^{(m)}}\mathcal{F}_R(k, n_f^{(s)}, n_f^{(m)})\right] \end{aligned} \tag{3.19}$$

JCAP03(2011)017

where $\tilde{k}^2 = k^2 + k_1^2 + 2kk_1\mu$ and the redshift independent integral is

$$\mathcal{F}_R(k, n_f^{(s)}, n_f^{(m)}) = \frac{1}{8\pi^2\sigma(M)^2}\int_0^\infty dk_1\; k_1^2 P_\Phi(k_1) M_R(k_1) \tag{3.20}$$
$$\times \int_{-1}^{1} d\mu\; M_R(\tilde{k}) \left[\frac{P_\Phi(\tilde{k})}{P_\Phi(k)} \left(\frac{k_1\tilde{k}}{k_p^2}\right)^{n_f^{(m)}} \left(\frac{k}{k_p}\right)^{n_f^{(s)}-n_f^{(m)}} \right.$$
$$\left. + \left(\frac{\tilde{k}}{k_p}\right)^{n_f^{(s)}} \left(\frac{k_1}{k_p}\right)^{n_f^{(m)}} + \frac{P_\Phi(\tilde{k})}{P_\Phi(k_1)} \left(\frac{k_1}{k_p}\right)^{n_f^{(s)}} \left(\frac{\tilde{k}}{k_p}\right)^{n_f^{(m)}} \right]$$
$$\to \frac{1}{2\pi^2\sigma(M)^2}\int_0^\infty dk_1\; k_1^2 P_\Phi(k_1) M_R^2(k_1) \left(\frac{k_1}{k_p}\right)^{n_f^{(s)}+n_f^{(m)}} .$$

The second expression is in the small k limit, so $\tilde{k} \approx k_1$. In that limit, $\mathcal{F}_R(k, n_f^{(s)}, n_f^{(m)})$ is a constant that depends on the smoothing scale. When $n_f^{(s),(m)} = 0$, this expression reduces to that of [92] and is identically one in the small k limit. Notice also that this agrees with the $\nu \gg 1$ result from the peak background split, eq. (3.16).

The Lagrangian halo bias b_L for halos of mass M is defined by

$$P_h(k) = b_L^2 P_\delta(k) = b_{L,0}^2 \left(1 + \frac{\Delta b}{b_{L,0}}\right)^2 P_\delta \tag{3.21}$$

where in the second equality the $f_{\rm NL} = 0$ contribution $b_{L,0}$ has been explicitly factored out. We will actually compare the halo-matter cross-correlation spectrum (rather than the halo auto-correlation) to the matter spectrum from our simulations, and so we are after an analytic expression for b itself instead of b^2. From eq. (3.19) the change in the bias relative to the Gaussian value is

$$\Delta b \approx \frac{\delta_c}{\sigma(M,z)^2} \left[\frac{2\delta_c}{M_R(k,z)} \xi_s(k_p)[\xi_m(k_p)]^2 \left(\frac{k}{k_p}\right)^{n_f^{(m)}} \mathcal{F}_R(k, n_f^{(s)}, n_f^{(m)}) \right] \tag{3.22}$$

where we have taken the square-root by expanding around the Gaussian result which is not always strictly valid. However, the resulting expression agrees with the peak background split (and we find that keeping the square-root yields worse agreement between theory and simulation). The results for the constant, small k part of the integral in eq. (3.20), $\mathcal{F}_R(k) \to \mathcal{F}(M, k \ll 1)$ for the representative two-parameter cases are plotted as a function of mass (related to smoothing scale R following eq. (3.7)) in figure 1. The functions $\xi_{s,m}$ are normalized to $\xi_{s,m}(k_p) = 1$ so that the left panel shows an effective $f_{\rm NL}$ generated by the scale-dependence for each scenario. The right panel compares the prediction for the non-Gaussian correction to the (Lagrangian) bias for the single-field and multi-field scenarios. (This label indicates how many fields contribute to the curvature perturbations - the inflaton itself may be separate).

3.4 Summary of analytic results

We have arrived at the same prediction in both of the previous subsections: a general factorizable and symmetric extension of the local ansatz leads to two possible modifications of

JCAP03(2011)017

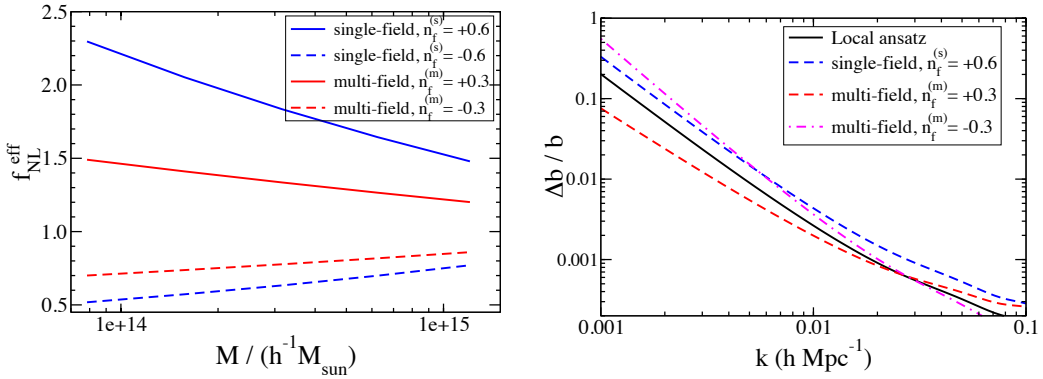

Figure 1. *Left panel*: The effective amplitude of the non-Gaussian bias on small scales ($f_{\rm NL}^{\rm eff}$) as a function of the object's mass for the generalized local ansatz with either $n_f^{(m)}$ or $n_f^{(s)}$ set to zero. The blue short dashed lines show the single field effect ($n_f^{(m)} = 0$) and the red long dashed lines show the multi-field function ($n_f^{(s)} = 0$). The upper lines show the effect of non-Gaussianity that increases on small scales, with $n_f^{(s)} = 0.6$ or $n_f^{(m)} = 0.3$ while the lower lines have $n_f^{(s)} = -0.6$ or $n_f^{(m)} = -0.3$. All curves are normalized to $\xi_{s,m}(k_p) = 1$. *Right panel*: A comparison of the correction to the bias of objects of mass $4.4 \times 10^{14}\ h^{-1}\, M_\odot$. The solid black curve is the usual local ansatz, the blue long dashed curve is the single-field model with $n_f^{(s)} = 0.6$, the red short dashed curve is the multi-field scenario with $n_f^{(m)} = 0.3$, and the purple dot-dashed curve is the multi-field scenario with $n_f^{(m)} = -0.3$. Again, $\xi_{s,m}(k_p) = 1$.

the non-Gaussian halo bias. First, different mass objects may see a different non-Gaussian correction that goes roughly like the amplitude of the non-Gaussianity on the scale of the object. Second, the power of k appearing in the scale-dependent correction can be shifted away from the standard k^{-2} result when there are two fields contributing to the curvature power and their relative importance is a function of scale. Either the first effect alone or a combination of both may be found, depending on the origin of the scale dependence. The most general case has two parameters to characterize the running, and one to characterize the amplitude. From the point of view of measurements of bias, these combine into the mass-dependent coefficient of the scale-dependent term, $f_{\rm NL}^{\rm eff}$, and the power of k that appears in the denominator. In other words, phenomenologically we have (in the small k limit)

$$\Delta b_{NG}(k, M) \propto \frac{f_{\rm NL}^{\rm eff}(M)}{k^{2-n_f^{(m)}}} \,. \tag{3.23}$$

More precisely (and in terms of the Gaussian Eulerian bias b_G^E)

$$\Delta b_{NG}(k, M) = f_{\rm NL}^{\rm eff}(M, n_f^{(s)}, n_f^{(m)}, k_p) \left(\frac{k}{k_p}\right)^{n_f^{(m)}} \left[\frac{3(b_G^E - 1)\delta_c \Omega_m H_0^2 g(\infty)}{c^2 k^2 T(k) D(z) g(0)}\right] \tag{3.24}$$

where

$$f_{\rm NL}^{\rm eff}(M, n_f^{(s)}, n_f^{(m)}, k_p) = \xi_s(k_p)[\xi_m(k_p)]^2 \mathcal{F}_R(k \ll 1, n_f^{(s)}, n_f^{(m)}) \,. \tag{3.25}$$

JCAP03(2011)017

There is some suggestion, both from simulations and from analytic considerations, that there is an additional factor multiplying the expression above for $\Delta b_{\rm NG}$ even in the case of constant local non-Gaussianity. For example, Giannantonio and Porciani [93] have suggested a multiplication by a factor

$$q = 1 + \frac{\Delta b_I}{b_G^E - 1} \tag{3.26}$$

where Δb_I is a second order non-Gaussian correction that can be calculated from some choice of non-Gaussian mass function (and the subscript I indicates that it is scale-independent). It corresponds to just the non-Gaussian part of their quantity b_{10} in, for example, their eq. (67).[5] Although this particular analytic expression is reasonably well motivated, we do not find that such a correction alone substantially improves the fit to our simulations (especially for negative $f_{\rm NL}$), so we remain agnostic about the analytic form of any additional corrections and instead focus on the effects unique to the generalized local form, especially $f_{\rm NL}^{\rm eff}(M)$. We have verified that for scale-independent local non-Gaussianity, the values of q fit from our simulations are consistent with the findings of Pillepich et al. [94], where q measured from their simulations is labeled β (see eq. (18) of that reference). From a practical perspective, the coefficient above can be fit from simulation and should not significantly affect our conclusions.

3.5 Forecasts based on the analytic prediction

We now estimate the ability of future observations to detect slow-roll values of the running parameter. Here we present Fisher matrix forecasts based on the analytic predictions above. This analysis complements earlier forecasts made for both the scale-independent [15, 25, 95, 96], and also scale-dependent [80] models of non-Gaussianity.

We first consider the two simpler scenarios, given in eq. (3.3), that isolate the single field or multi-field effects and each have only two parameters. These can be obtained by setting either of the functions ξ_s or ξ_m to one in the general expressions above (and so either $n_f^{(s)}$ or $n_f^{(m)}$ is set to zero). The explicit expressions are

$$\begin{aligned}
\text{single field}: \quad \Delta b_{\rm NG}(k,M) &= f_{\rm NL}^{\rm eff}(M, n_f^{(s)}, k_p) \left[\frac{3(b_G^E-1)\delta_c \Omega_m H_0^2 g(\infty)}{c^2 k^2 T(k) D(z) g(0)}\right] \\
f_{\rm NL}^{\rm eff}(M, n_f^{(s)}, k_p) &= \frac{\xi_s(k_p)}{2\pi^2 \sigma(M)^2} \int_0^\infty dk_1 \; k_1^2 P_\Phi(k_1) M_R^2(k_1) \; \left(\frac{k_1}{k_p}\right)^{n_f^{(s)}} \\
\text{multi}-\text{field}: \quad \Delta b_{\rm NG}(k,M) &= f_{\rm NL}^{\rm eff}(M, n_f^{(m)}, k_p) \left(\frac{k}{k_p}\right)^{n_f^{(m)}} \left[\frac{3(b_G^E-1)\delta_c \Omega_m H_0^2 g(\infty)}{c^2 k^2 T(k) D(z) g(0)}\right] \\
f_{\rm NL}^{\rm eff}(M, n_f^{(m)}, k_p) &= \frac{\xi_m(k_p)^2}{2\pi^2 \sigma(M)^2} \int_0^\infty dk_1 \; k_1^2 P_\Phi(k_1) M_R^2(k_1) \; \left(\frac{k_1}{k_p}\right)^{n_f^{(m)}}
\end{aligned} \tag{3.27}$$

We have used only the small k portion of the integral expression from eq. (3.20) since this corresponds to the prediction from the peak-background split, and since the integrand at high wavenumbers (e.g. $k \sim \mathcal{O}(0.1)\, h\,{\rm Mpc}^{-1}$) depends on the explicit form of the window function. We report constraints on the momentum dependent functions that contribute to

[5] We thank Tommaso Giannantonio for detailed correspondence on this point.

JCAP03(2011)017

the integral in $f_{\rm NL}^{\rm eff}(M)$:

$$\begin{aligned}
\text{most general}: \quad & f_{\rm NL}(k) = \xi_s(k_p)[\xi_m(k_p)]^2 \left(\frac{k}{k_p}\right)^{n_f^{(s)}+n_f^{(m)}} \\
\text{single field only}: \quad & f_{\rm NL}(k) = \xi_s(k_p) \left(\frac{k}{k_p}\right)^{n_f^{(s)}} \\
\text{multi}-\text{field only}: \quad & f_{\rm NL}(k) = [\xi_m(k_p)]^2 \left(\frac{k}{k_p}\right)^{n_f^{(m)}}
\end{aligned} \tag{3.28}$$

where the last two lines specialize to the simpler cases of considering only the single-field or multi-field effects. Conceptually, $f_{\rm NL}^{\rm eff}(M)$ and its Fourier-space analogue, $f_{\rm NL}(k)$ capture the *high frequency* scale-dependence of non-Gaussianity, $k \sim M^{-1/3}$. In addition to this, the bias has low-frequency scale-dependence $\propto k^{-2+n_f^{(m)}}$ for $k \ll M^{-1/3}$. This is why our expressions for $f_{\rm NL}(k)$ and $f_{\rm NL}^{\rm eff}(M)$ contain only one power of $n_f^{(m)}$, even though the bispectrum has two $k^{n_f^{(m)}}$ terms. Fiducial values adopted were $f_{\rm NL}(k_p) \equiv \xi_s(k_p)\xi_m^2(k_p) = 30$ (corresponding to the approximate central value of constant $f_{\rm NL}$ inferred from WMAP data [26]), and $n_f^{(s),(m)} = 0$ while $k_p = 0.04\,{\rm Mpc}^{-1}$ as before. We will see in a moment that the true best-measured scale from the large-scale clustering of galaxies and clusters is somewhat smaller.

Suppose that we have measurements of the power spectrum using objects (galaxies and clusters of galaxies) that have been separated in several mass bins. We assume that the covariance matrix of measured Fourier-space overdensities in a given redshift bin centered at z is given by

$$C_{ab}(k,z) = b(k,M_a,z)\,b(k,M_b,z)\,P(k,z) + \delta_{ab}\,\frac{1}{n_a(z)} \tag{3.29}$$

where the labels a and b refer to mass bins. This equation encodes how to combine observations from different mass bins, and also straightforwardly specifies the dependence on the parameters of interest $f_{\rm NL}^{\rm eff}(k_p)$ and $n_f^{(s),(m)}$ via eqs. (3.22) and (3.20).

The Fisher matrix can now be evaluated in the FKP approximation [97], where information is summed over the redshift bins and wavenumber shells. We have

$$F_{ij} = \Omega_{\rm survey} \int_0^{z_{\rm max}} \left(\frac{dV}{d\Omega dz}\right) dz \int_{k_{\rm min}}^{k_{\rm max}} {\rm Tr}\left[C^{-1}C_{,i}C^{-1}C_{,j}\right] \frac{k^2 dk}{(2\pi)^2}, \tag{3.30}$$

where $\Omega_{\rm survey}$ and $z_{\rm max}$ are the solid angle and maximum redshift in the survey respectively, V is volume, commas denote derivatives with respect to the non-Gaussian parameters, and we have suppressed the dependencies of C on wavenumber and redshift. In practice we replace integrals with sums to evaluate this expressions. We neglect the effect of redshift uncertainties, but assume thick redshift bins with $\Delta z = 0.2$.

For definiteness, we assume a dataset of the quality expected from the Dark Energy Survey (DES; [6]), with $z_{\rm max} = 1$ and covering 5000 square degrees; the total volume in this survey is about $6.5\,h^{-1}{\rm Mpc}^3$. We assume $k_{\rm min} = 0.0001\,h\,{\rm Mpc}^{-1}$ and $k_{\rm max} = 0.1\,h\,{\rm Mpc}^{-1}$; the latter ensures that all information safely comes from the linear regime. Although the largest scales included here are superhorizon, they contribute very little information to the final constraint because there are so few modes. However, to be precise on those scales one needs to specify a gauge, with comoving-orthogonal gauge recovering the expression used here [98]. Finally, we choose the number density of sources above some mass

JCAP03(2011)017

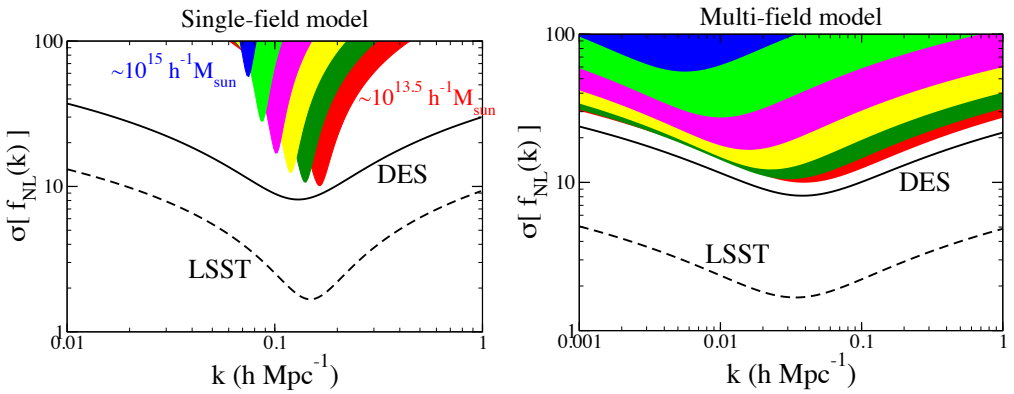

Figure 2. Forecasted constraints on $f_{\rm NL}(k)$ in the model where a single field generates the curvature perturbations (*left panel*) and in the multi-field model (*right panel*). We show forecasts for data expected from DES (solid black curve) and LSST (dashed black curve) observations. The wavenumber at which the constraints are the best is $k_{\rm uncorr}$, and at this wavenumber the normalization and slope of the power law are precisely uncorrelated. The six colored contours on top of each panel show the individual constraints from six narrow mass bins uniformly distributed in $\log_{10} M$ from $10^{13.5}\,h^{-1}M_\odot$ to $10^{15}\,h^{-1}M_\odot$ (assuming the DES survey). In the single-field scenario, individual masses do not break degeneracy between amplitude and running of $f_{\rm NL}(k)$ and only constrain this function at a single k value; combined masses are required to break the degeneracy. In the multi-field scenario, the degeneracy is broken even with halos of a fixed mass. [Note that, in all cases, the overall constraints on $f_{\rm NL}(k)$ between different wavenumbers k are strongly correlated, given that we are assuming a power law in k.]

to correspond exactly to the expectation from the Jenkins mass function [99]. Therefore, $n_a(z) = \int_{M_{a,\rm low}}^{M_{a,\rm high}} (dn/d\ln M)(z)\, d\ln M$, where $M_{a,\rm low}$ and $M_{a,\rm high}$ and the boundaries of the a-th mass bin. The total number density of sources at $z = 0$ and above $10^{13.5}\,h^{-1}M_\odot$ is $n \simeq 10^{-4}\,(h\,{\rm Mpc}^{-1})^{-3}$. We assume a large number of mass bins (forty) in $M/M_\odot$, uniformly distributed in $\log_{10} M$ from $10^{13.5}\,h^{-1}M_\odot$ to $10^{15.5}\,h^{-1}M_\odot$.

First considering the single-field case, the error in $f_{\rm NL}(k)$ at any k is given by a simple propagation of errors

$$\sigma(f_{\rm NL}(k)) = \left[\left(\frac{\partial f_{\rm NL}(k)}{\partial f_{\rm NL}(k_p)}\right)^2 {\rm Cov}_{\rm ff} + \left(\frac{\partial f_{\rm NL}(k)}{\partial n_f^{(s)}}\right)^2 {\rm Cov}_{\rm nn} + 2\frac{\partial f_{\rm NL}(k)}{\partial f_{\rm NL}(k_p)}\frac{\partial f_{\rm NL}(k)}{\partial n_f^{(s)}}{\rm Cov}_{\rm nf}\right]^{1/2} \tag{3.31}$$

$$= \left[\left(\frac{k}{k_p}\right)^2 n_f^{(s)} {\rm Cov}_{\rm ff} + \left(f_{\rm NL}(k_p)\left(\frac{k}{k_p}\right)^{n_f^{(s)}} \ln\left(\frac{k}{k_p}\right)\right)^2 {\rm Cov}_{\rm nn}\right. \tag{3.32}$$

$$\left. + 2 f_{\rm NL}(k_p)\left(\frac{k}{k_p}\right)^{2n_f^{(s)}} \ln\left(\frac{k}{k_p}\right) {\rm Cov}_{\rm nf}\right]^{1/2}$$

where ${\rm Cov} \equiv F^{-1}$ is the covariance matrix of the two non-Gaussian parameters that we consider. The errors in $f_{\rm NL}(k)$ are shown in the left panel of figure 2.

JCAP03(2011)017

We are also interested in finding the best-constrained wavenumber, $k_{\rm uncorr}$. When $k_p = k_{\rm uncorr}$, then the errors on the parameters $\xi(k_p)$ and $n_f^{(s),(m)}$ are uncorrelated . While this best-constrained wavenumber can obviously be read off from figure 2, it can also be calculated analytically as

$$k_{\rm uncorr} = k_p \exp\left(-\frac{{\rm Cov}_{\rm nf}}{f_{\rm NL}(k_p){\rm Cov}_{\rm ff}}\right), \tag{3.33}$$

where $k_p = 0.04\,h\,{\rm Mpc}^{-1}$ is the arbitrary pivot in eq. (3.2). The way that $k_{\rm uncorr}$ 'runs' with changing mass illustrates the point we made in section 3.2 that different mass halos probe scale-dependent NG on scales corresponding to those masses.

We find that the best-constrained wavenumber of our survey, for the single-field model and assuming DES-quality data, is $k_{\rm uncorr} \simeq 0.1\,h\,{\rm Mpc}^{-1}$, and the corresponding parameter errors at $k_{\rm uncorr}$ are

$$\sigma(f_{\rm NL}(k_{\rm uncorr})) \simeq 8, \quad \sigma(n_f^{(s)}) \simeq 0.5 \qquad ({\rm DES\ forecast,\ single-field}). \tag{3.34}$$

We also find that the error in $f_{\rm NL}(k_{\rm uncorr})$ is largely insensitive to the fiducial value of $f_{\rm NL}(k_p)$, while the error in the spectral index $n_f^{(s)}$ becomes larger for a smaller fiducial $f_{\rm NL}(k_p)$ (which is expected, since a larger fiducial non-Gaussianity increases the absolute change in $f_{\rm NL}(k \neq k_{\rm uncorr})$ for a fixed change in $n_f^{(s)}$).

We repeated the same exercise assuming data of the quality expected from the Large Synoptic Survey Telescope (LSST; [9]), with $z_{\rm max} = 3$ and covering 20,000 square degrees; the constraints became

$$\sigma(f_{\rm NL}(k_{\rm uncorr})) \simeq 1.7, \quad \sigma(n_f^{(s)}) \simeq 0.17 \qquad ({\rm LSST\ forecast,\ single-field}). \tag{3.35}$$

Next we consider the multi-field model; see the right panel of figure 2. As expected, the numerical constraints on the amplitude are comparable to the single-field case, however the constraints on the running improve, and the best-determined scale moves to a slightly lower k:

$$\sigma(f_{\rm NL}(k_{\rm uncorr})) \simeq 8, \qquad \sigma(n_f^{(m)}) \simeq 0.2 \qquad ({\rm DES\ forecast,\ multi-field}) \tag{3.36}$$

$$\sigma(f_{\rm NL}(k_{\rm uncorr})) \simeq 1.7, \quad \sigma(n_f^{(m)}) \simeq 0.04 \qquad ({\rm LSST\ forecast,\ multi-field}). \tag{3.37}$$

The colored contours in figure 2 show the individual constraints from each of the six narrow mass bins uniformly distributed in $\log_{10} M$ from $10^{13.5}\,h^{-1}M_\odot$ to $10^{15}\,h^{-1}M_\odot$ (this is for the DES survey scenario and the single-field inflaton model).[6] The thick black curve in either panel shows the combined constraint. Note that the combined constraint contains the information from the individual bins *and* the correlations between them (corresponding to $a \neq b$ in eq. (3.29)). A particularly interesting feature of testing these models with primordial non-Gaussianity is that halos of different mass complement in producing the overall constraint. For example, inspection of eqs. (3.22) and (3.20) shows that, with a single mass measurement, the normalization and slope of the single-field model, $f_{\rm NL}(k_p)$ and $n_f^{(s)}$, are completely degenerate, and only $f_{\rm NL}(k)$ at a single k value is measured. By adding a

[6] The careful reader will notice that these six bins in mass are an oversampling of the 30 original bins in mass we assumed in this interval, which are a subset of the total of 40 bins in mass we assumed in $M = [10^{13.5}, 10^{15.5}]\,h^{-1}M_\odot$.

JCAP03(2011)017

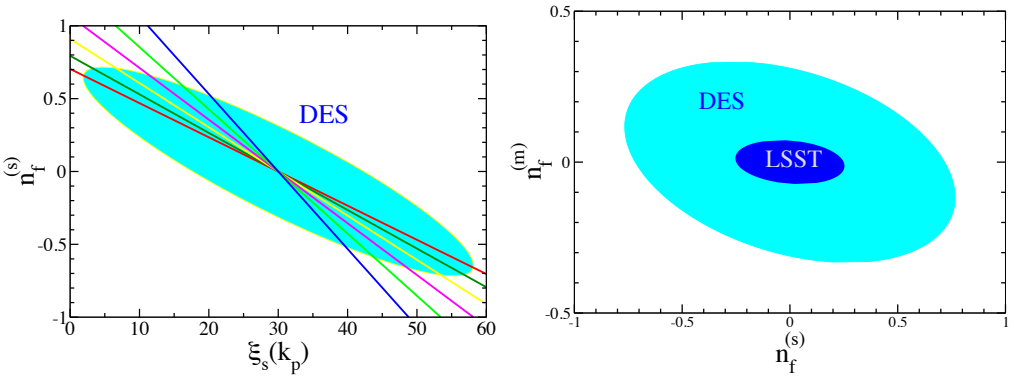

Figure 3. *Left panel:* constraints in the $f_{\rm NL}(k_p)$-$n_f^{(s)}$ plane in the inflaton model. Lines show degeneracy directions that each of six individual mass bins suffers (these mass bins correspond to colored curves in figure 2). *Right panel:* Constraints in the $n_f^{(s)}$-$n_f^{(m)}$ plane assuming both single-field and multi-field models, and marginalizing over the amplitude (term $f_{\rm NL}(k_p) \equiv \xi_s(k_p)\xi_m(k_p)^2$ in eq. (3.28)).

wide range of masses, this degeneracy is broken. This is shown in the left panel of figure 2, where narrow mass bins only constrain this function near a single k value. In contrast, the right panel shows that for the multi-field scenario the degeneracy is broken even with halos of a fixed mass, as expected from eq. (3.24).

Similarly, figure 3 contains more visual information on how the degeneracy is broken with multiple mass measurements. The left panel shows the constraint in the $f_{\rm NL}(k_p)$-$n_f^{(s)}$ plane for the DES survey, with lines showing degeneracy directions that each of the six individual mass bins suffers (these mass bins correspond to colored curves in figure 2). The right panel shows the constraint in the $n_f^{(s)}$-$n_f^{(m)}$ plane, marginalized over the amplitude $f_{\rm NL}(k_p) \equiv \xi_s(k_p)\xi_m(k_p)^2$, for both DES and LSST surveys.

Clearly, even the information from large-scale structure alone offers the possibility of distinguishing the origin of primordial non-Gaussianity by constraining both single-field and multi-field model parameters simultaneously, but the most interesting level to probe is running of order the spectral index, $n_f^{(s,m)} \sim \mathcal{O}(0.04)$. It is not completely clear if we can reach that level, and there are several factors that could push the predictions above in either direction. First, the forecasts presented here are in some sense a best-case scenario, given that for simplicity we did not marginalize over the standard cosmological parameters, and we assumed no systematic errors in recovering the power spectra of halos, only taking into account the statistical uncertainties. In particular, measurements of mass of clusters of galaxies suffer from statistical and systematic errors that are currently at least at the 10% level per cluster. On the other hand, constraints presented might be reached in the near future because we do not expect that serious degeneracies exist between the non-Gaussian and other cosmological parameters [15]. One exception might be the Gaussian bias b_G^E, which will need to be measured concurrently rather than predicted by theory as we assumed here.

In addition, we caution that our simulation results do not agree quantitatively with the analytic prediction (see the next section). In fact, the simulations find a substantially *stronger* dependence on mass than what is predicted. If the simulations are proven correct,

JCAP03(2011)017

then the effects shown above will be easier to distinguish, which is very encouraging for distinguishing between different mechanisms that may lead to large local non-Gaussianity.

Finally, the constraints above are from bias alone, but the Planck satellite will considerably improve constraints on $f_{\rm NL}$ from the CMB through measurements of the bispectrum itself, so that any scale dependence may also be constrained [80]. Whereas current constraints come from $k \simeq 10^{-3}\,h^{-1}$Mpc, Planck constraints will extend to higher ℓ and should overlap with constraints from the bias. Existing CMB analyses [80] have used a different parametrization of possible scale-dependence, and so it would be interesting to repeat this with our ansatz. As pointed out by [71] and explored in detail by [100], even more information can be extracted from joint constraints on models where two fields contribute to the curvature fluctuation. Multiple observations can separate the inherent size of the non-Gaussian interaction in one field ($f^{\sigma}_{\rm NL}$) from the rescaling by the fraction of power from the non-Gaussian field, $\xi(k)$, which combine as shown in eq. (2.16) to give the amplitude of the non-Gaussian term in the bias, $\xi^2_m(k) = f^{\sigma}_{\rm NL}\xi^2(k)$, that we have constrained here.

4 Simulation results

To check the dependence of the effective $f_{\rm NL}$ on the tracer mass, we generated initial conditions with a non-zero bispectrum of the form shown in the first line of eq. (3.3) (the single field model) with scale-dependent amplitude as defined in eq. (3.2). This is equivalent to eq. (3.4), so our function $\xi_s(k)$ corresponds to a commonly used definition for $f_{\rm NL}(k)$ (see also eq. (3.28)). This is the simplest possible model, but serves to check the predictions for how the effective coefficient of the non-Gaussian bias ("$f^{\rm eff}_{\rm NL}$") varies with the mass of the halo. We have also performed a small number of simulations using the bispectrum form in the second line of eq. (3.3), to verify that the bias has the expected scale-dependence. These simulations confirm that in such models Δb no longer simply scales as k^{-2} on large scales, but has $n_f^{(m)}$ dependence as well. However, at large enough values of the running to be distinguished by our simulations, second order effects are significant. For now we focus on the first scenario which is simpler and already uncovers a disagreement between the analytic predictions and the numerical results.

To perform these non-Gaussian simulations, we first generated a realization of a Gaussian random field $\Phi(x)$ with amplitude chosen so that $\sigma_8 = 0.8$ and with spectral index $n_s = 0.96$. Then we squared the field, Fourier transformed and multiplied by the scale-dependent $f_{\rm NL}$ shown in the second line of eq. (3.28). Finally, we transformed this component back to real space and added it to the Gaussian piece. We then use the Zeldovich approximation to initialize our particles at scale factor $a = 0.005$. We evolved the particles forward in a flat ΛCDM cosmology with parameters consistent with WMAP7 best fit values ($\Omega_m = 0.27$, $h = 0.7$), using a particle-mesh code with adaptive (drift-kick-drift) timestepping, and 8 grid cells per particle. We ran a Friends-of-Friends halo finder, using linking length $b = 0.2$, at $a = 0.5$, 0.667, and 1. We measure halo clustering and halo bias, using the large-scale ratio of the halo-matter cross-correlation function to the matter auto-correlation function.

We ran 8 realizations each of Gaussian and non-Gaussian initial conditions, including $\xi_s(k_p) \equiv f_{\rm NL}(k_p) = 100$ with $n_f^{(s)} = 0, 0.6$, $f_{\rm NL}(k_p) = 300$ with $n_f^{(s)} = 0, \pm 0.6$, and $f_{\rm NL}(k_p) = 630$ with $n_f^{(s)} = 0, -0.6$. All cases had pivot point $k_p = 0.04$ Mpc^{-1}. The box size was 2400 h^{-1} Mpc, with $(1024)^3$ particles, giving a mass per particle of $9.65 \times 10^{11} h^{-1} M_\odot$. Although our lowest-mass halos do not have many particles in these simulations, we used

JCAP03(2011)017

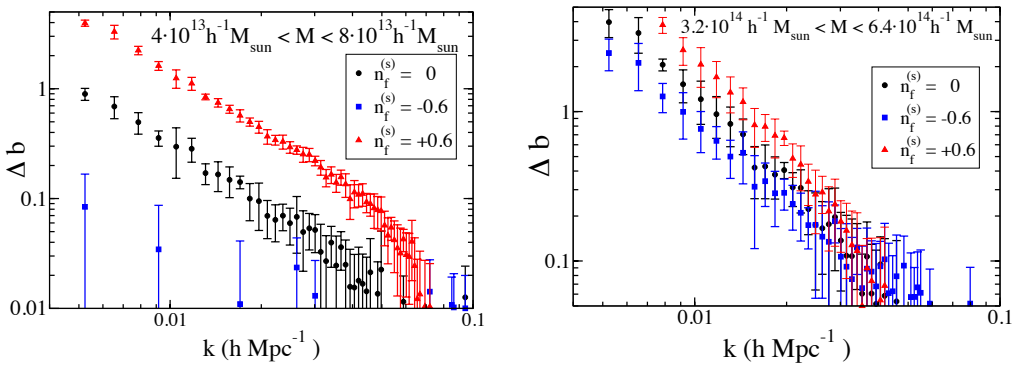

Figure 4. Dependence of scale-dependent non-Gaussian bias on mass, inferred from simulations. *Left panel*: Simulation results for the non-Gaussian contribution to the bias of halos with mass $(4-8)\times 10^{13}h^{-1}\,M_\odot$. The black circles points have constant $\xi_s(k_p) \equiv f_{\rm NL}(k_p) = 300$, the blue squares have the same $\xi_s(k_p)$ but $n_f^{(s)} = -0.6$, and the red triangles have $n_f^{(s)} = 0.6$. Error bars are sample variance across several simulations with the same parameters. *Right panel*: The same set of curves for halos with mass $(32-64)\times 10^{13}h^{-1}\,M_\odot$. The scatter here is larger than in the previous plot since there are fewer objects at this mass.

a few $L_{\rm box} = 520h^{-1}\,$Mpc simulations (with $f_{\rm NL}(k_p) = 300$) where these halos were well-resolved to verify our results. These simulations were performed on the SciNet machines, where each run took about 3.5 hours on 16 nodes.

We find that the simulations with constant $f_{\rm NL}$ are offset from the analytic expectation at small k by a factor that is nearly constant with mass and is less than one for both positive and negative $f_{\rm NL}$. This is consistent with findings by other simulations, and the behavior of the offset was studied in detail by Pillepich et al. [94] and Giannantonio and Porciani [93]. However, as discussed above, we will effectively fit this offset out and examine only the difference in behavior between our $f_{\rm NL}$ constant simulations and those with running.

From the simulations with scale-dependent non-Gaussianity, we find that different mass objects are indeed sensitive to an effective $f_{\rm NL}$ that depends on the scale of the object and which increases (decreases) for positive (negative) running as the mass and size of the object decreases. Figure 4 illustrates this effect: the non-Gaussian term in the bias for small mass objects has a smaller (larger) amplitude for positive (negative) running than for constant $f_{\rm NL}$ (left hand panel). The curves converge for larger mass objects (right hand panel). The bias correction Δb is calculated from the difference between the matter-halo cross correlation in a Gaussian simulation and the non-Gaussian case built from the same Gaussian realization, then averaged over realizations. The qualitative effect we expected is present, but for some halos the magnitude of the effect is not well predicted by the analytic expressions from section 3. Figure 5 shows the deviation between simulation and prediction for $f_{\rm NL} = 300$, $n_f^{(s)} = \pm 0.6$ (the same generic trend was seen in all parameter sets). We plot the ratio of the non-Gaussian correction with running to the non-Gaussian correction for constant $f_{\rm NL}$:

$$\mathcal{F}^{\rm sim} \equiv \frac{b(f_{\rm NL}=300, n_f^{(s)}=0.6) - b(f_{\rm NL}=0)}{b(f_{\rm NL}=300, n_f^{(s)}=0) - b(f_{\rm NL}=0)} = \frac{\Delta b(n_f^{(s)})}{\Delta b(n_f^{(s)}=0)}\,. \tag{4.1}$$

This is compared with the theoretical expectation calculated from the small k limit of

JCAP03(2011)017

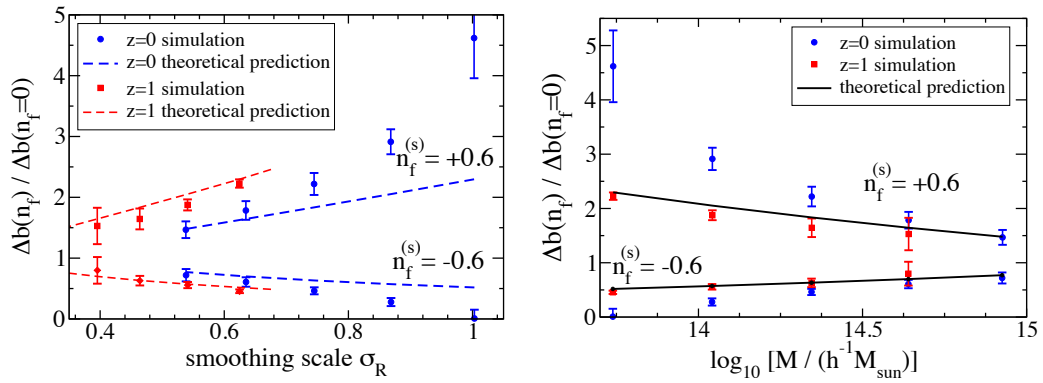

Figure 5. Simulation results for the scale-dependent non-Gaussian bias compared to theory. In the *left panel*, the vertical axis shows the mass-dependent ratio of the bias for non-Gaussianity that runs compared to the $f_{\rm NL}$ constant case, measured from $f_{\rm NL} = 300$ simulations at $z = 0$. The upper points/lines have $n_f^{(s)} = 0.6$ and lower points/lines show $n_f^{(s)} = -0.6$. Redshifts $z = 0$ (blue, higher values of $\sigma(M)$,and $z = 1$ (red, lower values of $\sigma(M)$ are shown. The dashed lines are the analytical prediction, showing that agreement is better at small $\sigma(M)$. The *right panel* shows the same information, but plotted as a function of mass. Note that the theoretical prediction as a function of mass (solid lines in the right panel) is redshift independent.

eq. (3.20). The curves are plotted as a function of $\sigma(M)$. As the figure demonstrates, the simulation results agree well with our analytic model in the high-mass limit $\sigma(M) \ll \delta_c$, but towards lower masses (e.g. $\sigma(M) \gtrsim 0.8$) the simulations produce a stronger effect than eq. (3.20) would predict. Note that the discrepancy does not appear at a fixed mass, but rather at a fixed $\sigma(M)$. This is illustrated in the right panel of figure 5, which is identical to the left panel of figure except that now mass M is the abscissa. The figure shows that for fixed mass M, the simulations agree with eq. (3.20) at high redshift, but begin to disagree at low redshift as $\sigma(M)$ grows.

One very plausible explanation for this discrepancy at low mass ($\sigma \gtrsim 0.8$) is that the profiles of the peaks that produce halos begin to change as σ increases. As we have argued, the non-Gaussian bias of halos of mass M is sensitive to the value of $f_{\rm NL}$ at some effective $k \propto M^{-1/3}$. Implicit in this scaling is the assumption that the profiles of peaks that collapse into halos are similar at different masses, just rescaled in size. However, we know that this assumption is incorrect. Bardeen et al. [89] argued from Gaussian statistics that as $\sigma(M)$ increases, the peaks that collapse into halos generally become steeper. N-body simulations confirm the presence of this effect, but show that it is much stronger in magnitude than predicted by Bardeen et al., apparently due to environmental effects during halo formation [101]. Because peaks at high $\sigma(M)$ are much steeper than rare peaks at low $\sigma(M)$, they are sensitive to non-Gaussianity at higher wavenumbers, even at the same peak size R. For scale-independent $f_{\rm NL}$, this change in peak profile has no effect, but for nonzero n_f it can dramatically enhance the mass dependence of non-Gaussianity, as our simulations show. It remains to be seen whether the magnitude of the change in peak profile can account for the discrepancy between our simulations and eq. (3.20); this is work in progress.

JCAP03(2011)017

5 Conclusions

In summary, we have introduced a generalization of the local ansatz, eq. (2.9), that is a symmetric, factorizable function of the momenta and includes scale-dependent non-Gaussianity. This more general expression is motivated by natural features of models that give an observably large amplitude for local type non-Gaussianity, and distinguishes between non-Gaussian curvature fluctuations generated by a single field and multiple fields. If only one field contributes to the curvature fluctuation (and is different from the inflaton so that the non-Gaussianity may be large), the scale-dependence of the non-Gaussianity characterizes the self-interactions of the field. If two fields contribute to the curvature fluctuations, scale-dependence indicates how the ratio of power in the fields changes, which is a function of how different the potentials are. If local non-Gaussianity is large enough to be observed, such scale-dependence is as natural as running of the power spectrum.

Models with scale-dependent local non-Gaussianity can generate two signatures in the non-Gaussian contribution to the halo bias. First, the non-Gaussian term may be proportional to an effective $f_{\rm NL}$ related to the amplitude of the bispectrum on the scale of the object so that different mass objects have a different amplitude correction. Second, the k^{-2} behavior of the non-Gaussian bias can be modified to $k^{-(2-n_f^{(m)})}$ (where $|n_f^{(m)}| < 1$), and one should expect the first effect to accompany this one.

We have used N-body simulations to verify that different mass objects do indeed have a non-Gaussian bias proportional to an effective $f_{\rm NL}$ that varies with the mass of the object. It is interesting that the simulations show that scale dependence with $n_f^{(s),(m)} < 0$ can erase the scale dependent effect on the bias for some range of masses, highlighting the need for analysis using multiple tracers of different mass. However, the quantitative result for halos at large $\sigma(M)$ is not well predicted by our analytic expressions. We have speculated that the origin of this discrepancy may be related to differences in the initial peak profiles of the halos, but leave a detailed investigation for a later work.

Future surveys are sure to bring interesting results. Using the analytic predictions, we find that they may be able to distinguish the different pieces of our generalized local ansatz, and so different origins of local non-Gaussianity, especially if the running is somewhat large ($n_f^{(s),(m)} \sim \mathcal{O}(0.1)$). However, the existing analytic expressions predict a *weaker* effect than we see in the simulations, and our forecasts only account for constraints from massive groups and clusters of galaxies, neglecting the (potentially) greater sensitivity to running possible when galaxy correlations are included as well. As we stressed throughout the paper, tracers of different masses can probe non-Gaussianity on distinct mass (and length) scales, so combining galaxy clustering measurements with measurements of groups and clusters should significantly improve upon the cluster-only constraints on running that we have presented. Our forecasts for future surveys should therefore be taken as a lower limit on the potential to observationally distinguish these features.

Acknowledgments

We thank Niayesh Afshordi, Carlos Cunha, Adrienne Erickcek, Louis Leblond, Fabian Schmidt, Roman Scoccimarro and especially Chris Byrnes for many very useful discussions and comments. We are grateful to Olivier Doré for collaboration in the early stages of this project, and for a careful reading of the manuscript. We also thank the Benasque Center for Physics for providing an excellent work environment for the last stages of this project,

JCAP03(2011)017

as well as the opportunity for discussions with Vincent Desjacques, Tommaso Giannantonio, Cristiano Porciani, and Emiliano Sefusatti. Computations were performed on the General Purpose Cluster at the SciNet HPC Consortium. SciNet is funded by the Canada Foundation for Innovation under the auspices of Compute Canada; the Government of Ontario; Ontario Research Fund - Research Excellence; and the University of Toronto. Research at the Perimeter Institute is supported in part by the Government of Canada through Industry Canada and by the Province of Ontario through the Ministry of Research and Information (MRI). DH is supported by the DOE OJI grant under contract DE-FG02-95ER40899, NSF under contract AST-0807564, and NASA under contract NNX09AC89G.

References

[1] C. Pitrou, J.-P. Uzan and F. Bernardeau, *The cosmic microwave background bispectrum from the non-linear evolution of the cosmological perturbations*, *JCAP* **07** (2010) 003 [arXiv:1003.0481] [SPIRES].

[2] E. Komatsu et al., *Non-Gaussianity as a Probe of the Physics of the Primordial Universe and the Astrophysics of the Low Redshift Universe*, arXiv:0902.4759 [SPIRES].

[3] *Planck Surveyor* — http://planck.esa.int.

[4] J.E. Carlstrom et al., *The 10 Meter South Pole Telescope*, arXiv:0907.4445 [SPIRES].

[5] *Baryon oscillation spectroscopic survey (boss)*, http://cosmology.lbl.gov/BOSS/.

[6] Dark Energy Survey collaboration, T. Abbott et al., *The dark energy survey*, astro-ph/0510346 [SPIRES].

[7] *Hobby eberly telescope dark energy experiment (hetdex)*, http://www.as.utexas.edu/hetdex/.

[8] *Physics of the accelerating universe (pau)*, http://www.ice.csic.es/research/PAU/PAU-welcome.html.

[9] *LSST* — http://www.lsst.org.

[10] X. Chen, *Primordial Non-Gaussianities from Inflation Models*, *Adv. Astron.* **2010** (2010) 638979 [arXiv:1002.1416] [SPIRES].

[11] N. Bartolo, S. Matarrese and A. Riotto, *Non-Gaussianity and the Cosmic Microwave Background Anisotropies*, arXiv:1001.3957 [SPIRES].

[12] M. Liguori, E. Sefusatti, J.R. Fergusson and E.P.S. Shellard, *Primordial non-Gaussianity and Bispectrum Measurements in the Cosmic Microwave Background and Large-Scale Structure*, *Adv. Astron.* **2010** (2010) 980523 [arXiv:1001.4707] [SPIRES].

[13] L. Verde, *Non-Gaussianity from Large-Scale Structure Surveys*, arXiv:1001.5217 [SPIRES].

[14] V. Desjacques and U. Seljak, *Primordial non-Gaussianity from the large scale structure*, *Class. Quant. Grav.* **27** (2010) 124011 [arXiv:1003.5020] [SPIRES].

[15] N. Dalal, O. Dore, D. Huterer and A. Shirokov, *The imprints of primordial non-Gaussianities on large-scale structure: scale dependent bias and abundance of virialized objects*, *Phys. Rev.* **D 77** (2008) 123514 [arXiv:0710.4560] [SPIRES].

[16] N. Kaiser, *On the Spatial correlations of Abell clusters*, *Astrophys. J.* **284** (1984) L9 [SPIRES].

[17] A. Slosar, C. Hirata, U. Seljak, S. Ho and N. Padmanabhan, *Constraints on local primordial non-Gaussianity from large scale structure*, *JCAP* **08** (2008) 031 [arXiv:0805.3580] [SPIRES].

[18] J.-Q. Xia et al., *Constraining Primordial Non-Gaussianity with High-Redshift Probes*, *JCAP* **08** (2010) 013 [arXiv:1007.1969] [SPIRES].

JCAP03(2011)017

[19] P. Creminelli and M. Zaldarriaga, *Single field consistency relation for the 3-point function*, *JCAP* **10** (2004) 006 [astro-ph/0407059] [SPIRES].

[20] D.S. Salopek and J.R. Bond, *Nonlinear evolution of long wavelength metric fluctuations in inflationary models*, *Phys. Rev.* **D 42** (1990) 3936 [SPIRES].

[21] L. Verde, L.-M. Wang, A. Heavens and M. Kamionkowski, *Large-scale structure, the cosmic microwave background and primordial non-Gaussianity*, *Mon. Not. Roy. Astron. Soc.* **313** (2000) L141 [astro-ph/9906301] [SPIRES].

[22] E. Komatsu and D.N. Spergel, *Acoustic signatures in the primary microwave background bispectrum*, *Phys. Rev.* **D 63** (2001) 063002 [astro-ph/0005036] [SPIRES].

[23] WMAP collaboration, E. Komatsu et al., *First Year Wilkinson Microwave Anisotropy Probe (WMAP) Observations: Tests of Gaussianity*, *Astrophys. J. Suppl.* **148** (2003) 119 [astro-ph/0302223] [SPIRES].

[24] M. Grossi, K. Dolag, E. Branchini, S. Matarrese and L. Moscardini, *Evolution of Massive Haloes in non-Gaussian Scenarios*, *Mon. Not. Roy. Astron. Soc.* **382** (2007) 1261 [arXiv:0707.2516] [SPIRES].

[25] C. Carbone, L. Verde and S. Matarrese, *Non-Gaussian halo bias and future galaxy surveys*, *Astrophys. J.* **684** (2008) L1 [arXiv:0806.1950] [SPIRES].

[26] WMAP collaboration, E. Komatsu et al., *Seven-Year Wilkinson Microwave Anisotropy Probe (WMAP) Observations: Cosmological Interpretation*, *Astrophys. J. Suppl.* **192** (2011) 18 [arXiv:1001.4538] [SPIRES].

[27] P. Creminelli, L. Senatore, M. Zaldarriaga and M. Tegmark, *Limits on f_{NL} parameters from WMAP 3yr data*, *JCAP* **03** (2007) 005 [astro-ph/0610600] [SPIRES].

[28] L. Senatore, K.M. Smith and M. Zaldarriaga, *Non-Gaussianities in Single Field Inflation and their Optimal Limits from the WMAP 5-year Data*, *JCAP* **01** (2010) 028 [arXiv:0905.3746] [SPIRES].

[29] P. Creminelli, A. Nicolis, L. Senatore, M. Tegmark and M. Zaldarriaga, *Limits on non-Gaussianities from WMAP data*, *JCAP* **05** (2006) 004 [astro-ph/0509029] [SPIRES].

[30] WMAP collaboration, D.N. Spergel et al., *Wilkinson Microwave Anisotropy Probe (WMAP) three year results: Implications for cosmology*, *Astrophys. J. Suppl.* **170** (2007) 377 [astro-ph/0603449] [SPIRES].

[31] G. Chen and I. Szapudi, *Constraining Primordial Non-Gaussianities from the WMAP2 2-1 Cumulant Correlator Power Spectrum*, *Astrophys. J.* **647** (2006) L87 [astro-ph/0606394] [SPIRES].

[32] N. Afshordi and A.J. Tolley, *Primordial non-Gaussianity, statistics of collapsed objects and the Integrated Sachs-Wolfe effect*, *Phys. Rev.* **D 78** (2008) 123507 [arXiv:0806.1046] [SPIRES].

[33] G.I. Rigopoulos, E.P.S. Shellard and B.J.W. van Tent, *Quantitative bispectra from multifield inflation*, *Phys. Rev.* **D 76** (2007) 083512 [astro-ph/0511041] [SPIRES].

[34] D. Seery and J.E. Lidsey, *Primordial non-Gaussianities from multiple-field inflation*, *JCAP* **09** (2005) 011 [astro-ph/0506056] [SPIRES].

[35] F. Vernizzi and D. Wands, *Non-Gaussianities in two-field inflation*, *JCAP* **05** (2006) 019 [astro-ph/0603799] [SPIRES].

[36] T. Battefeld and R. Easther, *Non-Gaussianities in multi-field inflation*, *JCAP* **03** (2007) 020 [astro-ph/0610296] [SPIRES].

[37] K.-Y. Choi, L.M.H. Hall and C. van de Bruck, *Spectral running and non-Gaussianity from slow-roll inflation in generalised two-field models*, *JCAP* **02** (2007) 029 [astro-ph/0701247] [SPIRES].

JCAP03(2011)017

[38] S. Yokoyama, T. Suyama and T. Tanaka, *Primordial Non-Gaussianity in Multi-Scalar Slow-Roll Inflation*, *JCAP* **07** (2007) 013 [arXiv:0705.3178] [SPIRES].

[39] S. Yokoyama, T. Suyama and T. Tanaka, *Primordial Non-Gaussianity in Multi-Scalar Inflation*, *Phys. Rev.* **D 77** (2008) 083511 [arXiv:0711.2920] [SPIRES].

[40] M. Sasaki, *Multi-brid inflation and non-Gaussianity*, *Prog. Theor. Phys.* **120** (2008) 159 [arXiv:0805.0974] [SPIRES].

[41] H.R.S. Cogollo, Y. Rodriguez and C.A. Valenzuela-Toledo, *On the Issue of the ζ Series Convergence and Loop Corrections in the Generation of Observable Primordial Non-Gaussianity in Slow-Roll Inflation. Part I: The Bispectrum*, *JCAP* **08** (2008) 029 [arXiv:0806.1546] [SPIRES].

[42] Y. Rodriguez and C.A. Valenzuela-Toledo, *On the Issue of the ζ Series Convergence and Loop Corrections in the Generation of Observable Primordial Non-Gaussianity in Slow-Roll Inflation. Part II: The Trispectrum*, *Phys. Rev.* **D 81** (2010) 023531 [arXiv:0811.4092] [SPIRES].

[43] C.T. Byrnes, K.-Y. Choi and L.M.H. Hall, *Conditions for large non-Gaussianity in two-field slow-roll inflation*, *JCAP* **10** (2008) 008 [arXiv:0807.1101] [SPIRES].

[44] C.T. Byrnes, K.-Y. Choi and L.M.H. Hall, *Large non-Gaussianity from two-component hybrid inflation*, *JCAP* **02** (2009) 017 [arXiv:0812.0807] [SPIRES].

[45] C.T. Byrnes, S. Nurmi, G. Tasinato and D. Wands, *Scale dependence of local f_{NL}*, *JCAP* **02** (2010) 034 [arXiv:0911.2780] [SPIRES].

[46] C.T. Byrnes and K.-Y. Choi, *Review of local non-Gaussianity from multi-field inflation*, *Adv. Astron.* **2010** (2010) 724525 [arXiv:1002.3110] [SPIRES].

[47] Q.-G. Huang, *Scale dependence of f_{NL} in N-flation*, *JCAP* **12** (2010) 017 [arXiv:1009.3326] [SPIRES].

[48] D.H. Lyth, C. Ungarelli and D. Wands, *The primordial density perturbation in the curvaton scenario*, *Phys. Rev.* **D 67** (2003) 023503 [astro-ph/0208055] [SPIRES].

[49] K. Ichikawa, T. Suyama, T. Takahashi and M. Yamaguchi, *Non-Gaussianity, Spectral Index and Tensor Modes in Mixed Inflaton and Curvaton Models*, *Phys. Rev.* **D 78** (2008) 023513 [arXiv:0802.4138] [SPIRES].

[50] M. Beltrán, *Isocurvature, non-Gaussianity and the curvaton model*, *Phys. Rev.* **D 78** (2008) 023530 [arXiv:0804.1097] [SPIRES].

[51] Q.-G. Huang, *Curvaton with Polynomial Potential*, *JCAP* **11** (2008) 005 [arXiv:0808.1793] [SPIRES].

[52] K. Enqvist, S. Nurmi, O. Taanila and T. Takahashi, *Non-Gaussian Fingerprints of Self-Interacting Curvaton*, *JCAP* **04** (2010) 009 [arXiv:0912.4657] [SPIRES].

[53] K. Enqvist and T. Takahashi, *Effect of Background Evolution on the Curvaton Non-Gaussianity*, *JCAP* **12** (2009) 001 [arXiv:0909.5362] [SPIRES].

[54] L. Alabidi, K. Malik, C.T. Byrnes and K.-Y. Choi, *How the curvaton scenario, modulated reheating and an inhomogeneous end of inflation are related*, *JCAP* **11** (2010) 037 [arXiv:1002.1700] [SPIRES].

[55] A. Chambers, S. Nurmi and A. Rajantie, *Non-Gaussianity from resonant curvaton decay*, *JCAP* **01** (2010) 012 [arXiv:0909.4535] [SPIRES].

[56] G. Dvali, A. Gruzinov and M. Zaldarriaga, *A new mechanism for generating density perturbations from inflation*, *Phys. Rev.* **D 69** (2004) 023505 [astro-ph/0303591] [SPIRES].

JCAP03(2011)017

[57] M. Zaldarriaga, *Non-Gaussianities in models with a varying inflaton decay rate*, *Phys. Rev.* **D 69** (2004) 043508 [astro-ph/0306006] [SPIRES].

[58] J. Kumar, L. Leblond and A. Rajaraman, *Scale Dependent Local Non-Gaussianity from Loops*, *JCAP* **04** (2010) 024 [arXiv:0909.2040] [SPIRES].

[59] M. Sasaki and E.D. Stewart, *A General analytic formula for the spectral index of the density perturbations produced during inflation*, *Prog. Theor. Phys.* **95** (1996) 71 [astro-ph/9507001] [SPIRES].

[60] D.H. Lyth and Y. Rodriguez, *The inflationary prediction for primordial non-Gaussianity*, *Phys. Rev. Lett.* **95** (2005) 121302 [astro-ph/0504045] [SPIRES].

[61] J.M. Maldacena, *Non-Gaussian features of primordial fluctuations in single field inflationary models*, *JHEP* **05** (2003) 013 [astro-ph/0210603] [SPIRES].

[62] C.T. Byrnes, M. Gerstenlauer, S. Nurmi, G. Tasinato and D. Wands, *Scale-dependent non-Gaussianity probes inflationary physics*, *JCAP* **10** (2010) 004 [arXiv:1007.4277] [SPIRES].

[63] S. Mollerach, *Isocurvature baryon perturbations and inflation*, *Phys. Rev.* **D 42** (1990) 313 [SPIRES].

[64] A.D. Linde and V.F. Mukhanov, *NonGaussian isocurvature perturbations from inflation*, *Phys. Rev.* **D 56** (1997) 535 [astro-ph/9610219] [SPIRES].

[65] T. Moroi and T. Takahashi, *Effects of cosmological moduli fields on cosmic microwave background*, *Phys. Lett.* **B 522** (2001) 215 [hep-ph/0110096] [SPIRES].

[66] K. Enqvist and M.S. Sloth, *Adiabatic CMB perturbations in pre big bang string cosmology*, *Nucl. Phys.* **B 626** (2002) 395 [hep-ph/0109214] [SPIRES].

[67] D.H. Lyth and D. Wands, *Generating the curvature perturbation without an inflaton*, *Phys. Lett.* **B 524** (2002) 5 [hep-ph/0110002] [SPIRES].

[68] C.T. Byrnes, K. Enqvist and T. Takahashi, *Scale-dependence of Non-Gaussianity in the Curvaton Model*, *JCAP* **09** (2010) 026 [arXiv:1007.5148] [SPIRES].

[69] Q.-G. Huang, *Negative spectral index of f_{NL} in the axion-type curvaton model*, *JCAP* **11** (2010) 026 [arXiv:1008.2641] [SPIRES].

[70] A.L. Erickcek, C.M. Hirata and M. Kamionkowski, *A Scale-Dependent Power Asymmetry from Isocurvature Perturbations*, *Phys. Rev.* **D 80** (2009) 083507 [arXiv:0907.0705] [SPIRES].

[71] D. Tseliakhovich, C. Hirata and A. Slosar, *Non-Gaussianity and large-scale structure in a two-field inflationary model*, *Phys. Rev.* **D 82** (2010) 043531 [arXiv:1004.3302] [SPIRES].

[72] D. Seery and J.E. Lidsey, *Non-Gaussianity from the inflationary trispectrum*, *JCAP* **01** (2007) 008 [astro-ph/0611034] [SPIRES].

[73] K. Ichikawa, T. Suyama, T. Takahashi and M. Yamaguchi, *Primordial Curvature Fluctuation and Its Non-Gaussianity in Models with Modulated Reheating*, *Phys. Rev.* **D 78** (2008) 063545 [arXiv:0807.3988] [SPIRES].

[74] D. Jeong and E. Komatsu, *Primordial non-Gaussianity, scale-dependent bias and the bispectrum of galaxies*, *Astrophys. J.* **703** (2009) 1230 [arXiv:0904.0497] [SPIRES].

[75] V. Desjacques and U. Seljak, *Signature of primordial non-Gaussianity of ϕ^3-type in the mass function and bias of dark matter haloes*, *Phys. Rev.* **D 81** (2010) 023006 [arXiv:0907.2257] [SPIRES].

JCAP03(2011)017

[76] P. Chingangbam and C. Park, *Statistical nature of non-Gaussianity from cubic order primordial perturbations: CMB map simulations and genus statistic*, *JCAP* **12** (2009) 019 [arXiv:0908.1696] [SPIRES].

[77] X. Chen, R. Easther and E.A. Lim, *Generation and Characterization of Large Non-Gaussianities in Single Field Inflation*, *JCAP* **04** (2008) 010 [arXiv:0801.3295] [SPIRES].

[78] A. Riotto and M.S. Sloth, *Strongly Scale-dependent Non-Gaussianity*, *Phys. Rev.* **D 83** (2011) 041301 [arXiv:1009.3020] [SPIRES].

[79] J. Khoury and F. Piazza, *Rapidly-Varying Speed of Sound, Scale Invariance and Non-Gaussian Signatures*, *JCAP* **07** (2009) 026 [arXiv:0811.3633] [SPIRES].

[80] E. Sefusatti, M. Liguori, A.P.S. Yadav, M.G. Jackson and E. Pajer, *Constraining Running Non-Gaussianity*, *JCAP* **12** (2009) 022 [arXiv:0906.0232] [SPIRES].

[81] A. Becker, D. Huterer and K. Kadota, *Scale-Dependent Non-Gaussianity as a Generalization of the Local Model*, *JCAP* **01** (2011) 006 [arXiv:1009.4189] [SPIRES].

[82] D.J. Eisenstein and W. Hu, *Power Spectra for Cold Dark Matter and its Variants*, *Astrophys. J.* **511** (1997) 5 [astro-ph/9710252] [SPIRES].

[83] N. Dalal, M. White, J.R. Bond and A. Shirokov, *Halo Assembly Bias in Hierarchical Structure Formation*, *Astrophys. J.* **687** (2008) 12 [arXiv:0803.3453] [SPIRES].

[84] B. Robertson, A. Kravtsov, J. Tinker and A. Zentner, *Collapse Barriers and Halo Abundance: Testing the Excursion Set Ansatz*, *Astrophys. J.* **696** (2009) 636 [arXiv:0812.3148] [SPIRES].

[85] S. Cole and N. Kaiser, *Biased clustering in the cold dark matter cosmogony*, *Mon. Not. Roy. Astron. Soc.* **237** (1989) 1127 [SPIRES].

[86] C. Wagner, L. Verde and L. Boubekeur, *N-body simulations with generic non-Gaussian initial conditions I: Power Spectrum and halo mass function*, *JCAP* **10** (2010) 022 [arXiv:1006.5793] [SPIRES].

[87] F. Schmidt and M. Kamionkowski, *Halo Clustering with Non-Local Non-Gaussianity*, *Phys. Rev.* **D 82** (2010) 103002 [arXiv:1008.0638] [SPIRES].

[88] R. Scoccimarro, L. Hui, M. Manera and K. Chan, in preparation.

[89] J.M. Bardeen, J.R. Bond, N. Kaiser and A.S. Szalay, *The Statistics of Peaks of Gaussian Random Fields*, *Astrophys. J.* **304** (1986) 15 [SPIRES].

[90] B. Grinstein and M.B. Wise, *Nongaussian Fluctuations and the Correlations of Galaxies or Rich Clusters of Galaxies*, *Astrophys. J.* **310** (1986) 19 [SPIRES].

[91] S. Matarrese, F. Lucchin and S.A. Bonometto, *A path-integral approach to large-scale matter distribution originated by non-Gaussian fluctuations*, *Astrophys. J.* **310** (1986) 21.

[92] S. Matarrese and L. Verde, *The effect of primordial non-Gaussianity on halo bias*, *Astrophys. J.* **677** (2008) L77 [arXiv:0801.4826] [SPIRES].

[93] T. Giannantonio and C. Porciani, *Structure formation from non-Gaussian initial conditions: multivariate biasing, statistics and comparison with N-body simulations*, *Phys. Rev.* **D 81** (2010) 063530 [arXiv:0911.0017] [SPIRES].

[94] A. Pillepich, C. Porciani and O. Hahn, *Universal halo mass function and scale-dependent bias from N-body simulations with non-Gaussian initial conditions*, arXiv:0811.4176 [SPIRES].

[95] B. Sartoris et al., *The potential of X-ray cluster surveys to constrain primordial non-Gaussianity*, arXiv:1003.0841 [SPIRES].

[96] C. Cunha, D. Huterer and O. Dore, *Primordial non-Gaussianity from the covariance of galaxy cluster counts*, *Phys. Rev.* **D 82** (2010) 023004 [arXiv:1003.2416] [SPIRES].

JCAP03(2011)017

[97] H.A. Feldman, N. Kaiser and J.A. Peacock, *Power spectrum analysis of three-dimensional redshift surveys*, *Astrophys. J.* **426** (1994) 23 [astro-ph/9304022] [SPIRES].

[98] D. Wands and A. Slosar, *Scale-dependent bias from primordial non-Gaussianity in general relativity*, *Phys. Rev.* **D 79** (2009) 123507 [arXiv:0902.1084] [SPIRES].

[99] A. Jenkins et al., *Mass function of dark matter halos*, *Mon. Not. Roy. Astron. Soc.* **321** (2001) 372 [astro-ph/0005260] [SPIRES].

[100] K.M. Smith and M. LoVerde, *Local stochastic non-Gaussianity and N-body simulations*, arXiv:1010.0055 [SPIRES].

[101] N. Dalal, Y. Lithwick and M. Kuhlen, *The Origin of Dark Matter Halo Profiles*, arXiv:1010.2539 [SPIRES].

JCAP03(2011)017